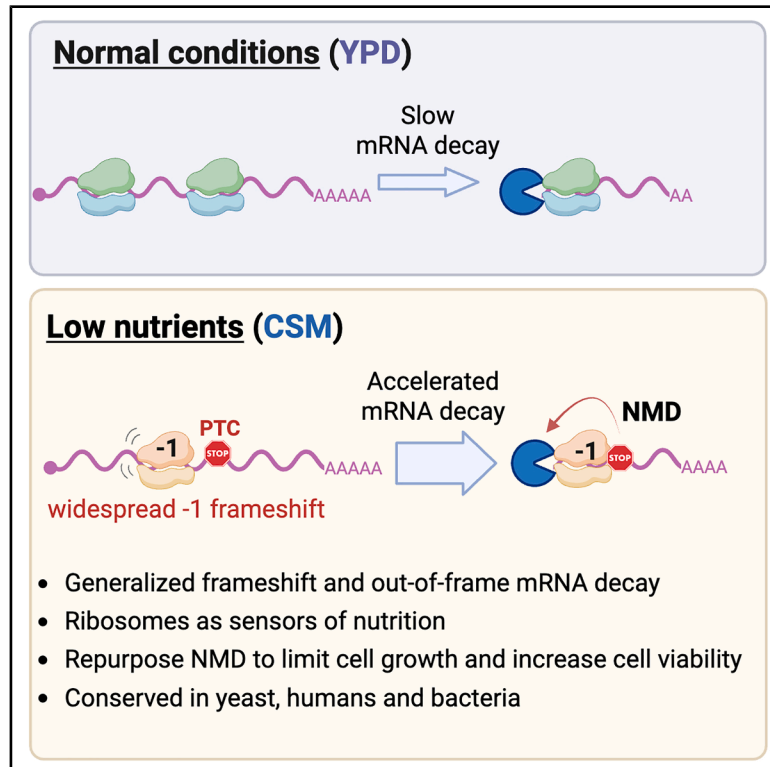


Ribosomes modulate transcriptome abundance via generalized frameshift and out-of-frame mRNA decay

Graphical abstract



Authors

Yujie Zhang, Lilit Nersisyan, Eliska Fürst, ..., Per Sunnerhagen, Ilaria Piazza, Vicent Pelechano

Correspondence

vicente.pelechano.garcia@ki.se

In brief

Zhang et al. identify a regulatory mechanism for how cells adapt to nutrient scarcity through widespread -1 ribosomal frameshifts, culminating in accelerated mRNA decay. This process, dependent on codon optimality and conserved across species, establishes direct feedback coupling the translation of new proteins with the stability of the mRNA that encodes for them.

Highlights

- Poor nutrition triggers -1 ribosome frameshifts and rapid mRNA decay in *S. cerevisiae*
- Low codon optimality modulates nutrition-induced frameshifts and mRNA decay
- Nutrition-induced frameshifts are conserved from bacteria to human
- Accelerated mRNA decay restricts growth under nutrient-poor condition



Article

Ribosomes modulate transcriptome abundance via generalized frameshift and out-of-frame mRNA decay

Yujie Zhang,¹ Lilit Nersisyan,^{1,2,3} Eliska Fürst,⁴ Ioannis Alexopoulos,¹ Carlos Santolaria,¹ Susanne Huch,¹ Claudio Bassot,⁴ Elena Garre,⁵ Per Sunnerhagen,⁶ Ilaria Piazza,⁴ and Vicent Pelechano^{1,7,*}

¹SciLifeLab, Department of Microbiology, Tumor and Cell Biology, Karolinska Institutet, Solna 171 65, Sweden

²Armenian Bioinformatics Institute, Yerevan, Armenia

³Institute of Molecular Biology, National Academy of Sciences of Armenia, Yerevan, Armenia

⁴Max Delbrück Center for Molecular Medicine in the Helmholtz Association (MDC Berlin), Berlin, Germany

⁵Department of Laboratory Medicine, Institute of Biomedicine, Sahlgrenska Academy, Sahlgrenska Center for Cancer Research, University of Gothenburg, 41390 Gothenburg, Sweden

⁶Department of Chemistry and Molecular Biology, University of Gothenburg 40530 Gothenburg, Sweden

⁷Lead contact

*Correspondence: vicente.pelechano.garcia@ki.se

<https://doi.org/10.1016/j.molcel.2025.04.022>

SUMMARY

Cells need to adapt their transcriptome to quickly match cellular needs in changing environments. mRNA abundance can be controlled by altering both its synthesis and decay. Here, we show how, in response to poor nutritional conditions, the bulk of the *S. cerevisiae* transcriptome undergoes –1 ribosome frameshifts and experiences an accelerated out-of-frame co-translational mRNA decay. Using RNA metabolic labeling, we demonstrate that in poor nutritional conditions, nonsense-mediated mRNA decay (NMD)-dependent degradation represents at least one-third of the total mRNA decay. We further characterize this mechanism and identify low codon optimality as a key factor for ribosomes to induce out-of-frame mRNA decay. Finally, we show that this phenomenon is conserved from bacteria to humans. Our work provides evidence for a direct regulatory feedback mechanism coupling protein demand with the control of mRNA abundance to limit cellular growth and broadens the functional landscape of mRNA quality control.

INTRODUCTION

The modulation of gene expression in response to evolving environmental conditions is fundamental for cellular survival. This adaptive capability holds particular significance for unicellular organisms such as budding yeast or bacteria, as they rely on precise adjustment in gene expression to thrive amidst changing surroundings. mRNA abundance depends on the fine balance between mRNA synthesis and decay, and mRNA decay controls the abundance of pre-existing mRNA molecules, modulates their availability for translation, and facilitates rapid transcriptomic changes.¹ Defects in mRNA decay have been associated with multiple diseases ranging from neurodegeneration² to viral infection,³ underscoring its significance in controlling gene expression.

Multiple mechanisms control mRNA decay in response to environmental changes, for example, by destabilizing specific mRNAs in response to RNA-binding proteins,⁴ by regulating the activity of proteins involved in mRNA decay,^{5,6} or through co-translational mRNA decay.^{7–9} A general process where the

translation process modulates mRNA decay is the coupling between the demand of tRNAs by translating ribosomes and the available supply of charged tRNAs (codon optimality), which has been shown to regulate mRNA stability.^{10–13} In addition to general processes controlling mRNA decay, multiple specialized mRNA surveillance pathways exist to ensure the elimination of faulty mRNAs and to facilitate ribosome recycling.^{12,14} Classic examples include the nonsense-mediated mRNA decay (NMD) pathway associated with the elimination of transcripts containing premature termination codons (PTCs)^{14–16} or the no-go decay (NGD) pathway associated with the removal of mRNAs with stalled ribosomes.¹¹ Importantly, in addition to eliminating faulty transcripts, those pathways can also modulate the abundance of canonical mRNAs.¹⁷ In general, NMD recognizes transcripts containing PTCs that can originate from genetic mutations, alternative splicing, or frameshifting events.¹⁴

Frameshifts can regulate mRNA stability by causing premature translation termination and thus recruiting the NMD machinery. The frequency of spontaneous ribosome frameshifts is usually very low, as it requires the presence of a slippery sequence



followed by a secondary structure element.^{18,19} Frameshifts can also occur during ribosome translocation via tRNA slippage at the P-site while the A-site is vacant,²⁰ especially associated with limitations in specific charged aa-tRNAs.¹⁹ While ribosomal frameshifts have previously been linked to the degradation of specific transcripts, it is unclear if those events play a significant role in controlling global mRNA abundance, particularly when considering that most genes do not contain putative programmed ribosomal frameshift (PRF) sites.^{21,22}

We have previously shown that during co-translational mRNA decay, 5'-3' exonucleases produce an *in vivo* toeprint of the position of the last (most 5') trailing ribosome in yeast⁸ and bacteria.⁹ Here, by investigating ribosome position associated with mRNA decay,^{8,23,24} we discovered that the bulk of the *S. cerevisiae* transcriptome (~77% of the degradation pool) undergoes -1 nt ribosome frameshifting in response to poor nutrient conditions. We characterize this process and identify both gene- and codon-specific features favoring frameshifting events. Next, we use genome-wide RNA metabolic labeling to demonstrate that in nutrient-poor conditions a sizable fraction of the transcriptome is degraded in an NMD-dependent manner. We further characterized this mechanism and showed that low codon optimality, rather than the presence of PRF sites or ribosome collisions, is central to this process and that amino acid supplementation can partially reverse this phenomenon. Next, we show that out-of-frame mRNA decay also contributes to changes in the proteome abundance. Surprisingly, this phenomenon is evolutionarily conserved and occurs not only in yeast and human cells but also in bacteria that lack canonical NMD machinery. Finally, we show that this mechanism restricts cellular growth and conserves limiting resources under low-nutrient conditions. We suggest that ribosome frameshifting followed by co-translational mRNA decay provides direct regulatory feedback coupling the demand of new proteins and the control of mRNA abundance encoding them.

RESULTS

Study of co-translational mRNA decay reveals generalized -1 ribosome frameshifts

Sequencing the 5' phosphate (5'P) mRNA degradation intermediates naturally present in cells with 5PSeq provides the *in vivo* position of the last translating ribosomes.⁸ Specifically, this technique relies on the fact that in budding yeast, the 5'-3' exonuclease Xrn1p follows the last translating ribosome, trimming the exposed 5'P ends *in vivo*. It differs from ribosome profiling, which uses *in vitro* RNase digestion to obtain footprints of all soluble ribosomes independent of whether the mRNAs are undergoing decay or not. 5PSeq is particularly well suited for investigating ribosome stalls associated with mRNA degradation because it produces a toeprint of the subset of ribosomes engaged in co-translational mRNA decay, unlike ribosome profiling, which instead studies the bulk of ribosomes present in the cell.^{23,24} In *S. cerevisiae*, ribosomes protect a region of 17 nt comprising the distance between the exposed 5'P of an mRNA undergoing degradation and the ribosome A-site. The ribosome-protected region at the 5' of mRNA has a constant size of 17 nt in different cellular conditions, such as during oxidative stress, heat shock, cycloheximide treatment, or different

growth media.^{8,24-26} However, we serendipitously discovered that in very poor nutritional conditions, the 17 nt ribosome protection pattern is displaced backward by 1 nt (-1 nt) (Figures 1A and S1A). When cells are grown in complete supplement medium (CSM), this apparent -1 frameshift can be clearly observed in the body of the genes but not close to the start codon (Figures 1B and 1C). In fact, the -1 nt displaced frame (F0) only becomes predominant around 400 nt from the start (Figure 1C, middle). However, we did not observe such alterations of the ribosome protection in other conditions with limited nutrients, such as cells depleted of glucose during early stationary phase or even using other synthetic defined media with slightly higher concentrations of nutrients (synthetic complete [SC] medium; see STAR Methods) (Figures S1B and S1C; Table S1). Long-term growth in CSM did not lead to disome accumulation (Figures S1D and S1E), suggesting that ribosome collisions do not drive the observed frameshifts as in other cases.²⁷

To explain the generalized -1 ribosome frameshift, we propose a working model where, under poor nutrient conditions, ribosomes undergo standard translation initiation but experience an increased frequency of -1 ribosome frameshift during translation elongation (Figure 1D). At the metagene level, this would cause a -1 frameshift to accumulate a few hundred nucleotides downstream of the start codon, in agreement with our observations (Figures 1B and 1C). Frequent ribosome frameshifts lead to the recognition of out-of-frame stop codons in the body of the genes and increased mRNA degradation via NMD. Reassuringly, we observed that putative out-of-frame stop codons increase 5PSeq ribosome footprints similar to those that we have previously described for canonical stop codons²⁴ in CSM but not in Yeast Peptone Dextrose medium (YPD) (Figure S1F).

Our model suggests the existence of two populations of mRNA degradation intermediates: a canonical population with in-frame co-translational degradation and a second population subjected to frameshift-dependent NMD-enhanced degradation after -1 frameshift. At the metagene level, and dependent on the relative importance of each pathway, we should observe canonical co-translational degradation profiles in the 5' region of the genes (before the frameshift event) and potentially altered protection (-1 frameshift) in the body of the genes (after the frameshift). This scenario is consistent with our observations (Figures 1 and S1) and suggests that the bulk of the degradome of cells growing in poor media arises from a frameshift-mediated degradation pathway.

Our working model also predicts that methods such as 5PSeq, focusing on transcripts undergoing decay, should easily identify frameshift events associated with mRNAs subjected to increased decay. By contrast, in methods such as ribosome profiling, footprints derived from non-frameshifted ribosomes over stable mRNAs would likely mask frameshift events (Figures S1G and S1H). This would also explain why the dramatic phenomenon that we describe here has not been reported before. To test this scenario, we performed ribosome profiling in CSM conditions. We observed a clear increase of out-of-frame reads in CSM, showing that ribosome frameshifting could also be detected using ribosome profiling (Ribo-seq) in the form of a -1 nt shoulder (Figures 1E, S1H, and S1I). However, the

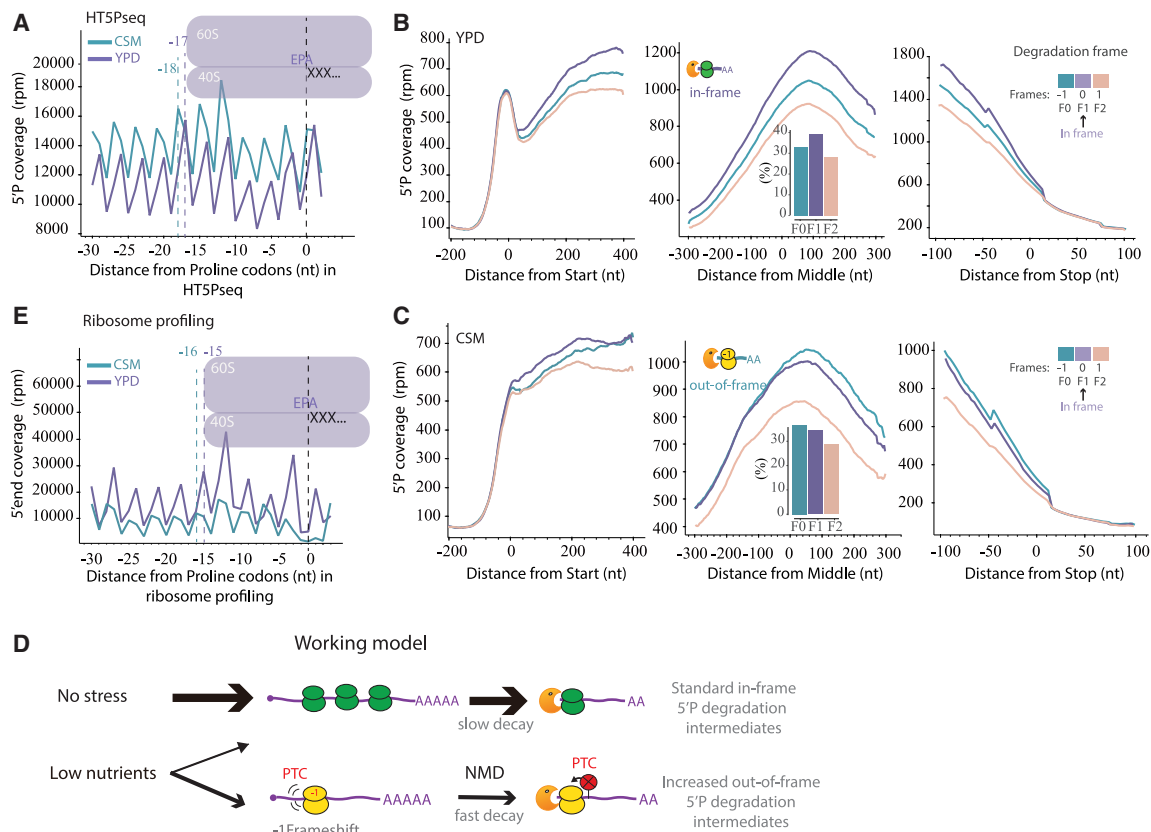


Figure 1. Study of co-translational mRNA decay reveals generalized -1 ribosome frameshifts

(A) Metagenome analysis displaying the abundance of 5'P reads coverage for all proline codons (CCG) across the transcriptome in YPD (in purple) and in CSM (in green) using HT-5Pseq. Dotted lines at -17 and -18 correspond to the *in-frame* and *out-of-frame* 5' end of protected ribosome located at the A-site, respectively. The same phenomenon can be seen for all codons. See Figure S1A.

(B) Relative 5'P coverage for each frame in YPD from around the start codon (left), the middle of genes (middle), and the stop codon (right). A histogram displaying the relative coverage for each protection frame is shown. In 5PSeq, standard *in-frame* decay displays an increased coverage for F1, while a -1 nt frameshift will lead to a relative increase of coverage for F0.

(C) Same as (B), but for CSM.

(D) Working model: in rich media conditions, *in-frame* mRNA degradation intermediates dominate the degradome. Under poor nutrient conditions, ribosomes will experience a higher frequency of -1 frameshifts. This will increase the proportion of *out-of-frame* mRNA degradation intermediates. mRNAs undergoing -1 frameshift would likely be degraded by NMD.

(E) Same as (A), but for ribosome profiling. Dotted lines at -15 and -16 correspond to the *in-frame* and *out-of-frame* distance of the 5' ends from the A-site of protecting ribosomes as measured after *in vitro* RNase digestion.

increase in *out-of-frame* protection measured by ribosome profiling was modest in comparison to the one measured by 5PSeq, where *out-of-frame* ribosome protection clearly dominates (Figure 1A). Importantly, the observed shoulder agrees with previous observations showing that NMD-regulated transcripts tend to have a higher ratio of *out-of-frame* reads.²⁸ Taking all this together, our results confirm the existence of environmentally regulated genome-wide ribosome frameshift events enriched in mRNAs undergoing co-translational decay.

Most genes experience environmentally induced -1 ribosome frameshifts

After showing the widespread existence of -1 frameshifts affecting the bulk of the transcriptome, we investigated the specificity of this process at the gene-specific level. We defined a simple metric to measure gene-specific frameshifts using the

3-nt periodicity associated with ribosome movement. For each gene, we compared the *in-frame* 5PSeq sequencing coverage with respect to the coverage for a -1 frameshift (i.e., $\log_2(F1/F0)$). Using this metric, only 212 genes (5.8 % of the 3,645 analyzed) present evidence for a -1 frameshift ($\log_2(F1/F0) < 0$) for exponentially growing cells in rich media (YPD) (Figures 2A and S2A; Table S2A). By contrast, for exponentially growing cells in CSM -1 frameshift-associated decay dominates the mRNA degradation in 2,804 genes (77% of analyzed) (Figures 2A and S2A; Table S2A). To corroborate this, we performed the same analysis using ribosome profiling. In ribosome profiling, the -1 frameshift is predominant for 34 genes in YPD (0.9%), and this number increases to 2,326 genes in CSM (58%) (Figure S2B). This result confirms our previous observation showing that 5PSeq provides higher resolution to investigate ribosome frameshifts associated with mRNA decay (Figures 1A and 1E). Next,

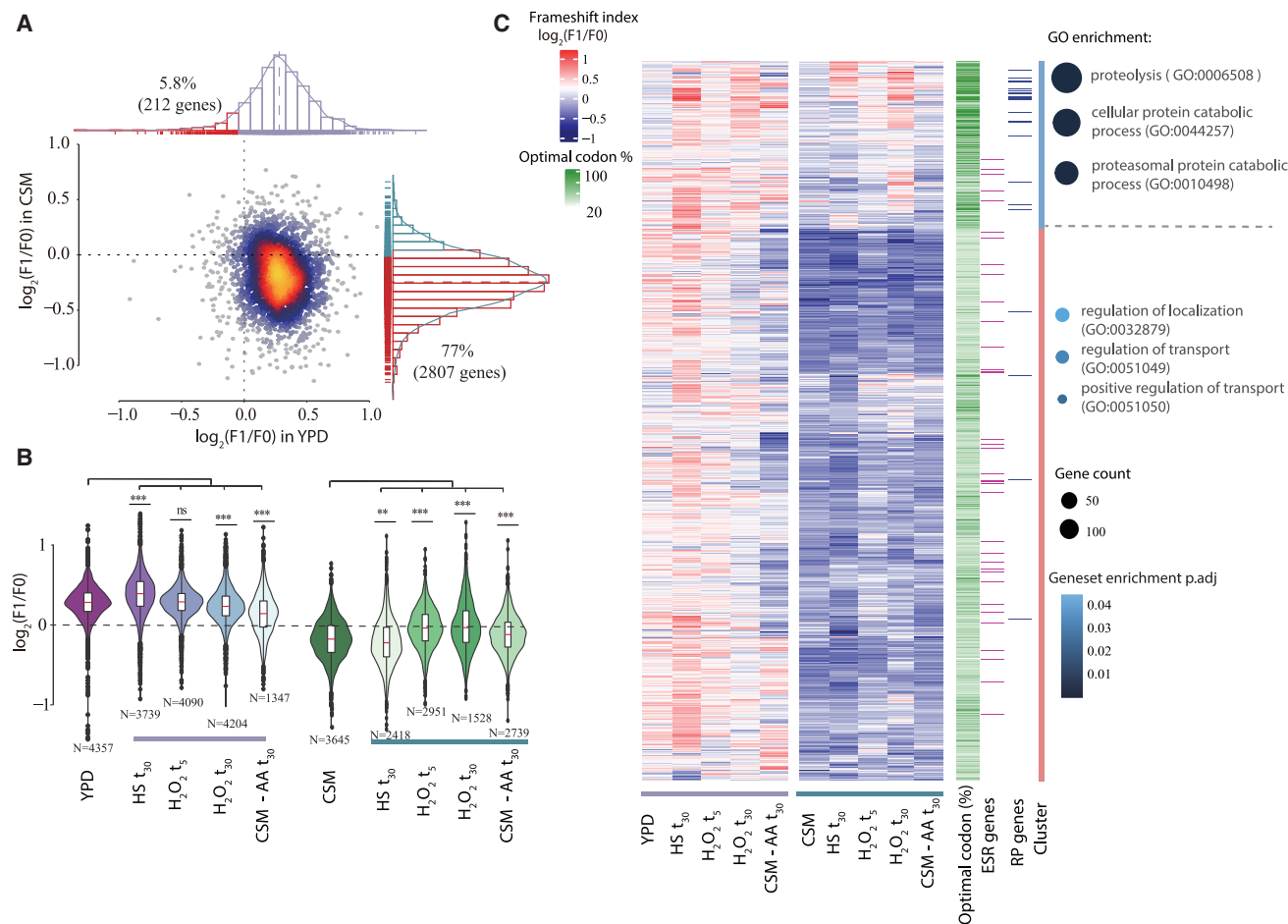


Figure 2. Gene-specific -1 ribosome frameshifts are environmentally regulated

(A) Scatterplot comparing the frameshift index $\log_2(F1/F0)$ for individual genes in rich (YPD, x axis) and poor (CSM, y axis) nutritional conditions. Histograms display the distribution of gene-specific frameshift indices. Genes dominated by *out-of-frame* decay ($\log_2(F1/F0) < 0$) are highlighted in red, namely 212 genes in YPD and 2,807 genes in CSM (5.8% and 77%, respectively, of total analyzed genes). Genes that were detected in all three replicates were considered for further analysis.

(B) Frameshift index distributions across tested conditions in YPD (left) and CSM (right). Stresses include heat shock at 42°C for 30 min (HS t_{30}), 0.2 mM H_2O_2 exposure for 5 or 30 min ($H_2O_2 t_5$ and $H_2O_2 t_{30}$), and amino acid deprivation (transfer to CSM lacking amino acids) for 30 min (CSM-AA t_{30}). The red line indicates the median gene frameshift index. Statistical analysis was performed using two-sided Wilcoxon rank-sum tests to its original condition (YPD and CSM) ($***p < 2.2 \times 10^{-16}$; $**p < 6.3 \times 10^{-9}$). The numbers of analyzed genes are displayed.

(C) Heatmap of frameshift index $\log_2(F1/F0)$ for genes detected under all tested conditions (as in B) starting from YPD (right) or CSM (left) clustered by k-means. Heatmap represents frameshift index $\log_2(F1/F0)$, red to blue. The percentages of optimal codons for each gene are shown in green. Environmental stress response (ESR)²⁹ genes and ribosomal protein genes are indicated in purple and blue, respectively. Frameshift index across all stress conditions were clustered using k-means (rightmost column). Gene ontology enrichment terms for high and low frameshifted gene clusters are displayed (p adj < 0.05).

we investigated if this -1 frameshift phenomenon was specific to exponential growth in poor nutrition or if it was induced also by other environmental challenges. To test these hypotheses, we investigated the effect of heat shock (30 min at 37°C), oxidative stress (5 and 30 min after 0.2 mM H_2O_2 addition), and amino acid deprivation for 30 min after growth in both rich and poor media (Figures 2B and S2C–S2J; Table S2B). Although the applied stressors differentially modulated the likelihood of frameshifts (as measured by the $\log_2(F1/F0)$ ratio), it was clear that the used growth medium was the main driver of the phenotype (Figure 2B).

We used the 5PSeq data generated across the 10 tested growth conditions to investigate gene-specific -1 frameshifts (Figure 2C). Genes associated with regulation of RNA localization and intracellular protein transport presented a higher degree of frameshifting, while this was less pronounced in genes associated with proteolysis (Table S2C). Ribosomal protein (RP) genes also had a relatively low tendency to experience an environment-dependent -1 ribosome frameshift (Figures 2C and S2K). As we saw that stress conditions can modulate the level of frameshifting, we also investigated the behavior of the environmental stress response (ESR) genes.²⁹ However, we did not

observe any clear association between the ESR genes and the frameshift events (Figure S2K).

Finally, we investigated if other gene-specific features could explain the observed differences in gene-specific frameshifting propensity. Factors, such as gene or UTR length, did not affect the observed differences (Figures S2L–S2R). However, GC content in the coding sequences (CDS) and especially lower codon optimality¹⁰ and lower mRNA stability were clearly associated with the gene-specific frameshifting sensitivity (Figures 2C, S2M, S2P, and S2Q). We found the association between lower codon optimality and increased frameshifts particularly interesting, as it suggests a direct role of the ribosomes in this process. Additionally, our working model suggests that mRNAs experiencing a higher level of frameshifting events will be mainly degraded by an NMD-dependent pathway (Figure 1D), consistent with the fact that NMD-regulated transcripts tend to have lower codon optimality scores.²⁸

Global frameshifting in poor nutritional conditions promotes mRNA decay

A central prediction of our model is the co-existence of two alternative co-translational mRNA degradation pathways: a canonical *in-frame* decay and an accelerated frameshift-dependent *out-of-frame* one (Figure 1D). To estimate the fraction of the transcriptome degraded by each pathway, we leveraged our 5PSeq data, which provides a snapshot of all mRNAs undergoing degradation. We used the conservative assumption that the fraction of *out-of-frame* transcripts in YPD is nearly 0%, and then simulated a dataset with a 100% theoretical *out-of-frame* decay (shifting all YPD reads by -1 nt). By mixing reads of these two datasets at varying ratios, we obtained a theoretical distribution of codon protection indexes, based on which we estimated that at least 52% of the degradome originates from *out-of-frame* decay in CSM (Figures 3A and 3B; Table S3A; see STAR Methods for details). This number is a very conservative estimate, as *out-of-frame* decay is not negligible in cells exponentially growing in YPD.

To test our model using an independent approach, we measured mRNA decay using pulse and chase RNA metabolic labeling followed by RNA sequencing (SLAM-seq).³⁰ This approach does not rely on the capture of transient mRNA degradation intermediates and measures the disappearance of mRNAs, independent of the decay occurring co-translationally or not. We incubated cells for 60 min in a medium containing 4-thiouracil (4tU) and measured mRNA prior (t_0) and after changing cells to a medium without 4tU after 15 and 30 min in both YPD and CSM (see STAR Methods for detail). Despite the known general association between faster cell growth and increased mRNA turnover in budding yeast,³¹ we observed an increased mRNA decay (lower mRNA stability) in CSM (Figure 3C), where cell growth is slower. This suggests that in CSM, in addition to the standard mRNA decay pathways associated with cell growth, another mechanism contributes to accelerated decay. As our previous results suggest that *out-of-frame* co-translational decay is associated with NMD, we compared the wild-type strain with an NMD-deficient strain (*upf1Δ*) (Figures 3D and S3B). In rich media, deletion of *UPF1* did not increase mRNA stability and, in

fact, led to a subtle increase in the mRNA degradation rate (suggesting potential adaptation of mRNA turnover in the *upf1Δ* strain). By contrast, in poor CSM conditions, deletion of *UPF1* led to an increased mRNA stability (decrease of mRNA degradation rate). This confirms that in nutritionally poor conditions (in CSM), NMD is actively degrading a big fraction of the transcriptome. Using the generated mRNA metabolic data, we fitted the labeled mRNA abundance (normalized to total library size) across time to a non-linear decay model equation to calculate degradation rate for each condition.³⁰ We estimated that in CSM the median NMD-dependent degradation rate (measured from *upf1Δ*, 1.87 min^{-1}) corresponds to at least 32% of the total decay rate (measured from wild type, 2.75 min^{-1}), while non-NMD-dependent degradation represents the remaining 68% (Figure 3D; Table S3C). Thus, even using conservative assumptions, under poor nutrition conditions at least one-third of the transcriptome is degraded via environmentally induced ribosome frameshifts.

Next, we investigated the changes in gene-specific mRNA stability for cells with and without *UPF1* in rich and poor media. We classified those genes experiencing an increased NMD-dependent decay in CSM as environmental *upf1*-sensitive genes (i.e., the 712 genes where degradation rate $(\text{WT}/\text{upf1}\Delta)_{\text{CSM}} > 1.2$ and $(\text{WT}/\text{upf1}\Delta)_{\text{YPD}} < 0.8$). Those genes were enriched for cell cycle and chromosome organization (Figure 3E; Table S3D). We then compared environmental NMD-sensitive genes with those experiencing environmentally induced frameshift ($\log_2(F1/F0)_{\text{YPD}} > 0.2$ and $\log_2(F1/F0)_{\text{CSM}} < -0.2$), see STAR Methods) and found a significant overlap (Figure 3F). Since a small fraction of -1 frameshift events will not lead to the downstream recognition of a PTC (e.g., those occurring close to the canonical stop codon), we classified genes according to the frequency and position of the expected PTC (Figures S3C–S3E). Reassuringly, genes where frameshift events are more likely to result in the downstream recognition of a PTC and subsequently trigger NMD showed increased NMD-dependent stabilization under CSM conditions (Figures 3G and S3E). Given the complex interplay between mRNA decay and translation,³² we investigated how frameshifting intersects with nutrient stress signaling (Gcn1), RNA decapping (Dcp2), and codon optimality-mediated decay (Dhh1) (Figures S3F and S3G; Table S3E). The *gcn1Δ* strain shows slower mRNA decay rates in CSM compared with wild-type cells, while it leads to a clear increase in mRNA degradation in YPD. The *gcn1Δupf1Δ* double also has slower decay rates in CSM. However, it shows an unexpected RNA stabilization relative to *gcn1Δ*. This indicates a possible interaction or compensatory mechanism between nutrition-dependent NMD and GCN1-mediated regulation and highlights the complexity of this interplay. Next, we assessed the interaction between NMD and decapping using a *dcp2Δ* strain. As expected, nutrition-regulated Dcp2-sensitive and Upf1-sensitive transcripts clearly overlap (Figure S3H). Finally, we tested the overlap with codon optimality-mediated decay using a *dhh1Δ* strain. Although *UPF1*-mediated NMD may function independently of codon optimality-mediated decay under rich nutrient conditions, our data suggest that in low-nutrition environments, *UPF1*-mediated NMD becomes indirectly dependent on codon optimality (see below). In agreement with our working model, nutrition-regulated Dhh1-sensitive and Upf1-sensitive transcripts

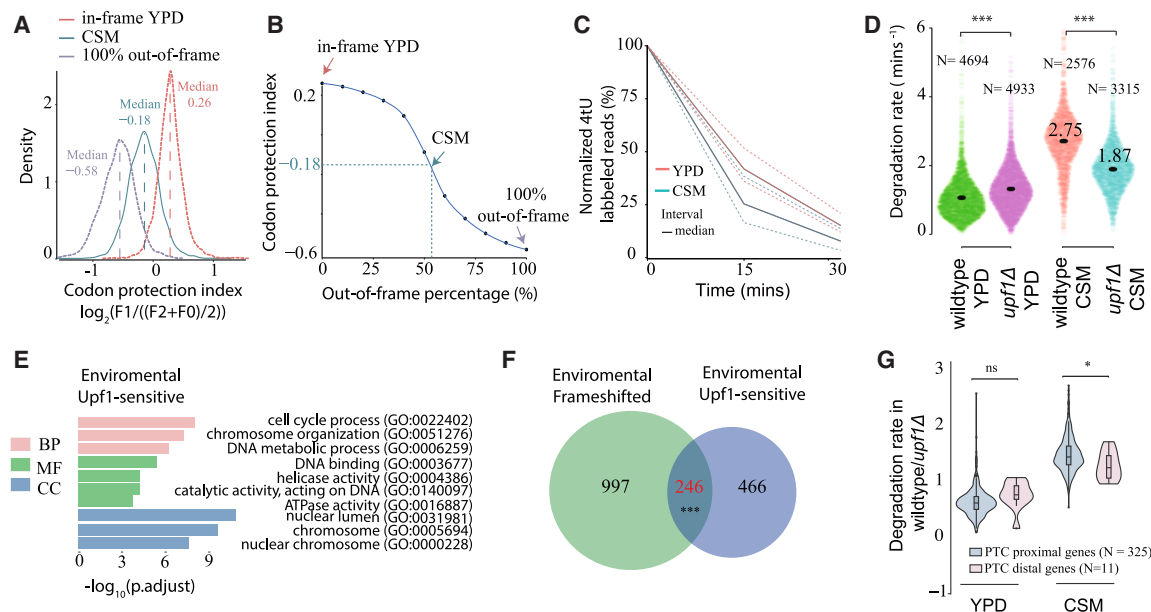


Figure 3. Ribosome frameshifts promote mRNA degradation in poor nutritional conditions

(A) Distribution of gene-specific codon protection index for cells in YPD (median 0.26, red), in CSM (median -0.18 , green), and simulated 100% *out-of-frame* decay (median -0.58 , purple). Codon protection index was calculated as the ratio of the reads corresponding to the protected frame (F1) with respect to the average number of reads of the non-protected frames: $\log_2(F1/(F2 + F0)/2)$.

(B) Relationship between median codon protection index (y axis) and percentage of *out-of-frame* reads (x axis). Data were generated by mixing different ratios of 0% and 100% *out-of-frame* decay (see STAR Methods). The green dotted line represents the median of codon protection index in CSM (-0.18) and corresponding estimated *out-of-frame* reads percentage (52%).

(C) Line plot displaying the average percentage of 4tU-labeled reads after 15 and 30 min 4tU pulse-chase. Data for YPD (pink) and CSM (green) are shown. Dotted lines provide the mean and median range.

(D) Violin plot comparing the median degradation rate (min^{-1}) for wild-type (BY4741) and NMD mutant (*upf1Δ*) both in YPD and CSM. Only coding mRNAs with at least 20 total reads are considered for RNA turnover analysis.

(E) Gene Ontology terms for genes classified as environmentally dependent Upf1-sensitive genes (degradation rate (wild type/*upf1Δ*)_{CSM} > 1.2 and (wild type/*upf1Δ*)_{YPD} < 0.8) in three aspects (BP, biological process; CC, cellular component; MF, molecular function). Only top enrichments are shown (p adj < 0.01). Gene set universe ($N = 5,375$) was set to the genes detected by SLAM-seq across all conditions (Table S3E).

(F) Overlap between genes subjected to environmentally dependent NMD decay (Upf1-sensitive) and genes showing environmentally dependent frameshifts ($\log_2(F1/F0)_{YPD} > 0.2$ and $\log_2(F1/F0)_{CSM} < -0.2$). Statistical analysis was performed by Fisher's exact test ($N = 5,375$) (Table S3E).

(G) Relative NMD-dependent (Upf1) stabilization in YPD and CSM. Genes are classified by the relative distance of the last -1 frameshift PTC to the canonical stop codon. PTC proximal genes (the last downstream -1 PTC occurs after $\geq 94\%$ of CDS length, and thus most frameshifts can lead to PTC recognition and NMD) and PTC distal genes (the last downstream -1 PTC occurs $\leq 60\%$ of CDS length, and only a fraction of frameshift events will engage NMD). Statistical analysis was performed using two-sided t tests. * $p = 0.019$.

overlap (Figure S3H). This finding is consistent with the fact that the influence of codon optimality on mRNA decay is modulated by cellular metabolic states and energy levels.³³ Taking all these observations together, we concluded that *out-of-frame* NMD-dependent degradation is responsible for the degradation of an important fraction of the transcriptome in poor nutritional conditions.

Codon optimality controls environmentally regulated -1 frameshifts and *out-of-frame* mRNA decay

After confirming the genome-wide nature of the environmentally regulated -1 frameshifts and their consequences for mRNA stability, we focused on their mechanisms. First, we investigated whether known mRNA slippery sequences^{21,22} caused the frameshifts. We reasoned that ribosome protection frames should be different before and after the ribosome encounters those regions if it was the case. However, we did not observe

any evidence for enhanced frameshifting surrounding slippery sequences (Figure S4A).

Since we observed massive frameshifts under poor nutrient conditions, it could be due to limited availability of charged tRNAs. This is a phenomenon previously described for specific codons or mRNAs^{34–36} named “hungry codon” frameshift.³⁷ To test if a similar mechanism could be operating at a genome-wide scale, we measured the degree of frameshift associated with each codon. We computed a relative protection frame for each codon (i.e., comparing 5PSeq coverage at -17 nt (F1, *in-frame*) and -18 nt (F0, *out-of-frame*) from the A-site; Figure 4A). Next, we compared the change in protection frame between YPD and CSM and defined a frameshift index such that codons more likely to induce a frameshift will present a higher value (i.e., $\log_2(F1/F0)_{YPD} - \log_2(F1/F0)_{CSM}$). This analysis revealed that codons with lower optimality were more likely to engage in frameshifting in poor nutritional conditions. To further

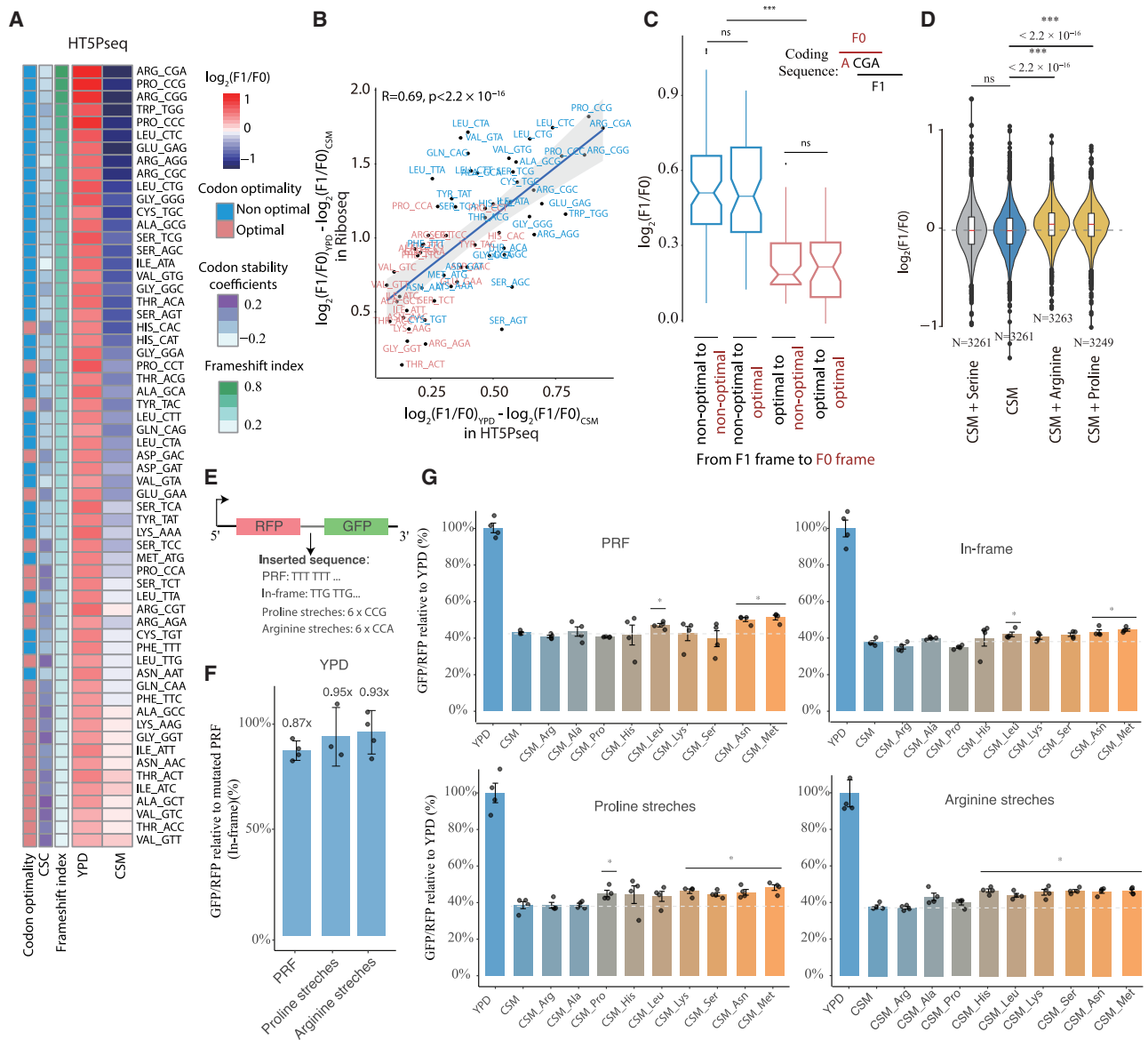


Figure 4. Codon optimality controls out-of-frame mRNA decay

(A) Heatmap comparing 5PSeq coverage at \log_2 ratio of -17 nt (F1) and -18 nt (F0) relative to the A-site of codons in YPD and CSM. The codons are ordered by the differences of frameshift index between YPD and CSM (i.e., $\log_2(F1/F0)_{\text{YPD}} - \log_2(F1/F0)_{\text{CSM}}$). Codon stability coefficients (CSCs) and codon optimality from Presnyak et al.¹⁰

(B) Scatterplot comparing frameshift index using HT-5PSeq and ribosome profiling. Spearman correlation is shown. Optimal codons and non-optimal codons are represented in red and blue, respectively.

(C) Boxplot comparing the frameshift index among different combinations. The four combinations include (1) non-optimal codons at both 17 nt (F1) and -18 nt (F0), (2) non-optimal codons at F1 and optimal codons at F0, (3) optimal codons at F1 and non-optimal codons at F0, and (4) optimal codons at both F1 and F0. Non-optimal codons at F1 (in frame) are represented by blue, and optimal codons at F1 are represented by red. Statistical analysis was performed using two-sided Wilcoxon rank-sum tests. $***p < 2.2 \times 10^{-16}$.

(D) Metagene plot showing the frameshift index change after amino acid supplementation. Serine, arginine, or proline were added to reach the comparable concentration as SC medium. Statistical analysis was performed using two-sided Wilcoxon rank-sum tests. $***p < 2.2 \times 10^{-16}$; ns, $p = 0.58$; Number of analyzed genes are displayed.

(E) Schematic diagram of the frameshift reporter construct, showing the frameshift test sequence inserted upstream of RFP and GFP coding regions.

(F) Effect of frameshift frequency in YPD using the reporter system. Data were normalized to the mutated PRF (in frame) as a control.

(G) Effect of various amino acid supplementation on frameshift frequency using the reporter system. Each amino acid was supplemented at a concentration of 85.6 mg/L. Data were normalized to YPD controls. Statistical significance was determined by t test comparing CSM with individual amino acid supplements ($*p < 0.05, n = 4$ biological replicates).

test this, we performed the same analysis using ribosome profiling data, which showed a similar trend ($R = 0.69$), albeit with less sensitivity (Figures 4B and S4B; Tables S4A and S4B). To investigate the impact of codon abundance at the gene-specific level, we compared the frameshift index distributions between YPD and CSM (Figure S4C) and focused on genes with high frameshift values ($\log_2(F1/F0)_{YPD} > 0.2$ and $\log_2(F1/F0)_{CSM} < -0.2$). We then calculated the Pearson correlation coefficient between the measured frameshift change (i.e., $\log_2(F1/F0)_{YPD} - \log_2(F1/F0)_{CSM}$) and codon occurrence among these genes (Figure S4D). Consistent with our expectations, we found a positive correlation between a high frameshift index and the abundance of non-optimal codons, while low frameshift values were associated with a greater prevalence of optimal codons. All these results agree with our previous observation that mRNAs with lower codon optimality tend to display more frameshifts in CSM conditions (Figures 2B and S2P). Finally, we reasoned that in those conditions where a rare codon was in the A-site and a -1 ribosome frameshift could lead to the incorporation of a common tRNA, the likelihood of frameshifting could increase. However, the nature of the incorporated codons after the frameshift played a minor role in this phenomenon (Figure 4C).

To experimentally validate if the continued low amino acid availability for cells growing exponentially in CSM was a key driver of the observed phenomenon, we raised the final concentration of selected amino acids in CSM to the one present in SC media (see STAR Methods). We first increased the concentration of amino acids whose codons are associated with a higher frequency of frameshifts: arginine and proline (from 50 to 85.6 mg/L and 0 to 85.6 mg/L, respectively). Reassuringly, both decreased the observed genome-wide frameshift events with respect to CSM (p value $< 2.2 \times 10^{-16}$) (Figures 4D and S4). While increased serine levels did not alter global frameshift patterns, they induced specific codon-level changes (Figures 4D and S4F), with non-optimal codons showing stronger responses to proline and arginine than to serine supplementation (Figure S4F). To further validate the role of amino acid availability in nutritionally induced frameshifts, we used an orthogonal approach. We designed a dual fluorescent reporter (red fluorescent protein [RFP]-linker-green fluorescent protein [GFP]) to measure frameshifting through GFP/RFP ratios (Figure 4E; Table S4). As in our conditions, frameshift events are not restricted to the linker region, and our system will detect any frameshift preventing the expression of a functional GFP (i.e., frameshifts occurring in the linker or the GFP CDS). We tested four linker sequences: a known PRF sequence,³⁸ its mutated version, and stretches of non-optimal codons (6xCCG proline or 6xCGA arginine). In agreement with expectations,^{38,39} the PRF derived from HIV-1 resulted in an increase of approximately 13% in frameshift frequency. While the linker sequences containing proline and arginine stretches did not clearly induce frameshift in rich YPD media (Figure 4F), all constructs exhibited ~50% lower GFP/RFP ratios (increased frameshift) in nutrient-limited conditions. This shows that in more than half of the translation events resulting in the production of a fully folded RFP, translation does not continue up to the point of yielding a functional GFP. Proline supplementation reduced frameshifting in

proline-rich linkers by 7%, while asparagine and methionine supplementation broadly suppressed frameshifting across all constructs (Figure 4G). This shows that long-term limitation in amino acid availability contributes to the appearance of genome-wide frameshifts and accelerates mRNA degradation. However, it is important to note that the reporter assay used does not directly measure -1 frameshifting and could be influenced by any other factor altering the measured GFP/RFP ratios.

Long-term amino acid limitation rewires the cellular proteome downstream of ribosome frameshifting

To further characterize the cellular state during conditions with high frameshifting, we analyzed the proteome of cells grown in CSM and YPD. We identified 487 proteins differentially expressed (Q value < 0.01), with 315 proteins significantly upregulated in CSM ($\log_2(\text{oldchange [FC]} > 1)$) and 172 proteins significantly downregulated ($\log_2(\text{FC} < -1)$) (Figure 5A; Table S5). Upregulated proteins involved mainly the proteasome complex, amino acid metabolic process, and ergosterol biosynthetic process (Figures 5B and S5A), supporting that cells grown in CSM have a limited availability of amino acids in the media and therefore need to upregulate the amino acid biosynthesis. Downregulated proteins were associated with components such as ribosomes, mitochondrial ribosomes, and nucleosomes, in agreement with the slower growth rate in CSM. To further investigate the role of amino acid-dependent translation repression,⁴⁰ we compared proteome changes between *gcn1Δ* and wild-type strains in different media (Figures S5B–S5D; Table S5). The proteome changes in CSM are likely influenced by multiple factors such as transcription regulation or slow growth. To focus on the downstream consequences of the frameshifts, we investigated if the observed frameshifts, in addition to modulating mRNA stability, also led to changes in protein abundance. We compared protein abundance changes for those genes experiencing a relatively high level of frameshift (i.e., 588 genes where $\log_2(F1/F0)_{YPD} > 0.2$ and $\log_2(F1/F0)_{CSM} < -0.2$ and proteins are detected [Q value < 0.01]) with those without frameshifts (362 genes where $\log_2(F1/F0)_{YPD \text{ and } CSM} > 0$). We observed that protein abundance for genes with a higher frameshifting decreases more drastically in CSM than the relative protein abundance for those genes without frameshifts (Figure 5C). All this confirms that, in addition to regulating the mRNA stability, this process also leads to differential protein abundance.

Generalized nutrition-induced frameshifts are evolutionarily conserved

Having characterized environmentally induced *out-of-frame* co-translational mRNA decay in *S. cerevisiae*, we explored the evolutionary conservation of this process. We reasoned those unicellular organisms, which are more exposed to the environment and need to adapt faster to changing conditions, should in principle be more susceptible to this phenomenon. As we have recently shown that 5'-3' co-translational mRNA decay is also frequent in bacteria,⁹ we investigated this process in *Lactobacillus plantarum*, where the 5'-3' exonuclease RNase J generates an *in vivo* toeprinting of the bacterial ribosome (14 nt from the A-site). We reanalyzed our previous data⁹ where *L. plantarum* was grown exponentially in rich (MRS broth) and

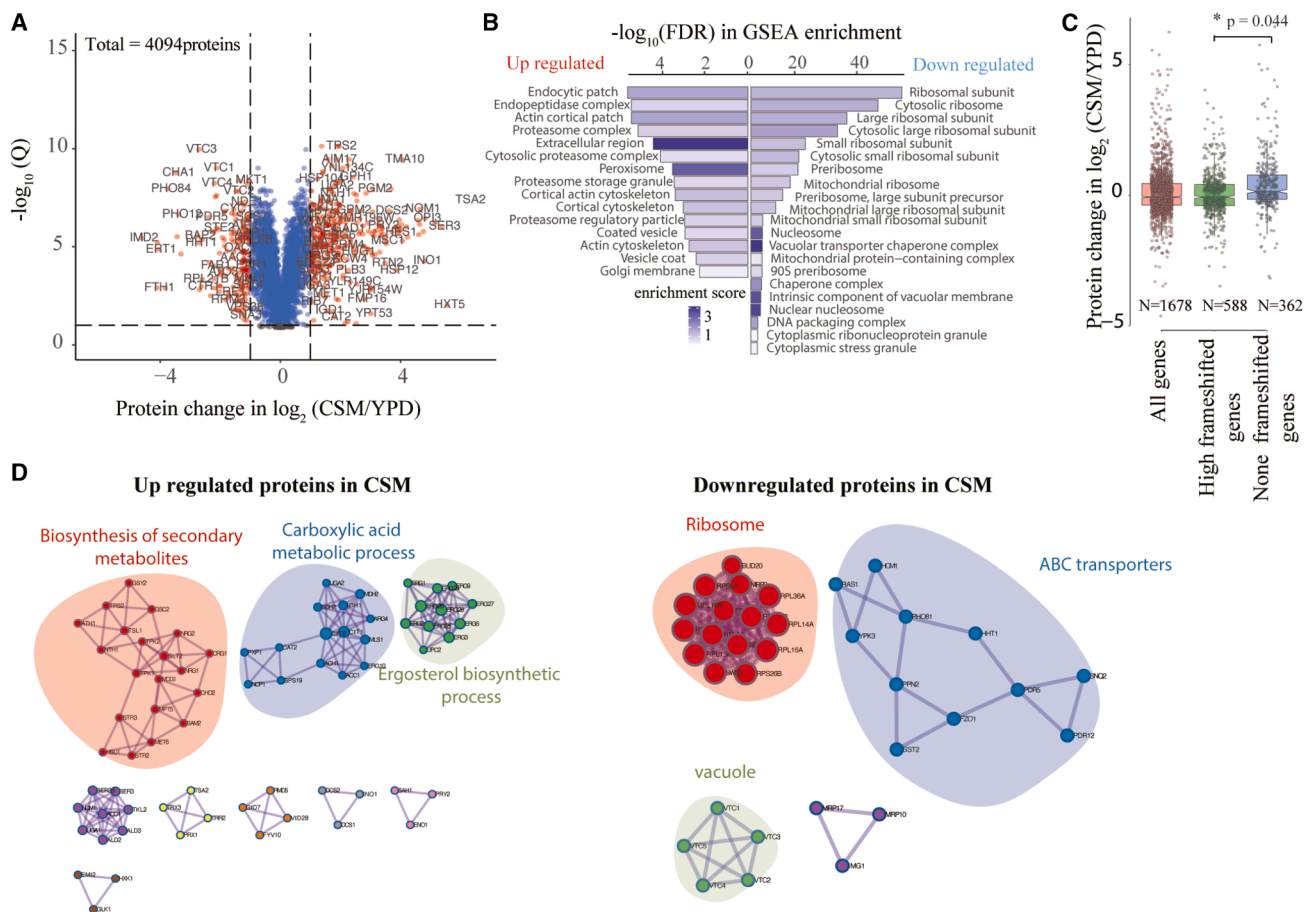


Figure 5. Long-term amino acid limitation rewires cellular proteome

(A) Volcano plot comparing protein abundance change between YPD and CSM in \log_2 fold change (x axis) versus the statistical significance ($-\log_{10}Q$). We used a threshold of Q value < 0.01 and $\log_2FC > 1$ or $\log_2FC < -1$ to define 315 upregulated and 172 downregulated proteins. Only proteins with at least 2 peptides were considered for analysis (4,094 proteins in total).

(B) Gene set enrichment analysis (GSEA) for differential protein abundance ranking according to \log_2 FC with ClusterProfiler using Fisher's exact test with p adjusted value < 0.05 .

(C) Boxplot comparing protein abundance levels for genes that are also detected in 5PSeq. Genes categorized as all genes ($N = 1,440$), high frameshifted genes ($\log_2(F1/F0)_{YPD} > 0.2$ and $\log_2(F1/F0)_{CSM} < -0.2$, $N = 496$ genes), and not frameshifted genes ($\log_2(F1/F0)_{YPD}$ and $CSM > 0$, $N = 319$ genes). Statistical analysis is performed using Wilcoxon rank-sum tests with p value < 0.05 .

(D) Upregulated and downregulated proteins highlighting their protein-protein interactions. Analysis was performed using performed metaspape v3.5. Only statistically significant enrichments are shown (p adj < 0.05).

transferred to low-nutrient media ($0.5 \times$ LB media, lysogeny broth) for 15 min. Despite the short exposure to low-nutrient conditions, we observed a significant increase for -1 frameshift ($\log_2(F1/F0) < 0$) events in 6% of genes, up from 2% (48 genes) under rich conditions (Figure 6A; Table S6).

To further test the conservation of this phenomenon at longer times, we investigated the 5'P degradome for *Bacillus subtilis*. Specifically, we compared the co-translational ribosome protection pattern for *B. subtilis* exponentially growing in rich (LB) and in poor media (minimal growth medium; see STAR Methods). Reassuringly, we observed a similar pattern where only 83 genes (3 % of measured) present evidence for -1 frameshifts in rich media, but this number increased to 336 genes (12%) in poor media (Figure 6B; Table S6). This pattern also held true when

we checked *B. subtilis* during early stationary phase (after 24 h growth in LB), where the number of genes dominated by -1 frameshifts increased to 17% of measured genes (Figure S6A). This shows that environmentally dependent *out-of-frame* co-translational mRNA decay that we described in budding yeast (Figure S4C) is also common in prokaryotes, even in the absence of NMD. To investigate if the -1 frameshift followed a similar mechanism to the one studied in eukaryotes, we analyzed the codon compositions of genes with varying susceptibility to frameshifting. Our findings, similar to those in yeast (Figure S4C), show a clear positive correlation between a high frameshift change (i.e., $\log_2(F1/F0)_{control} - \log_2(F1/F0)_{treatment}$) and a high occurrence of non-optimal codons among genes with frameshifts ($\log_2(F1/F0)_{control} > 0$ and $\log_2(F1/F0)_{treatment} < 0$) and vice

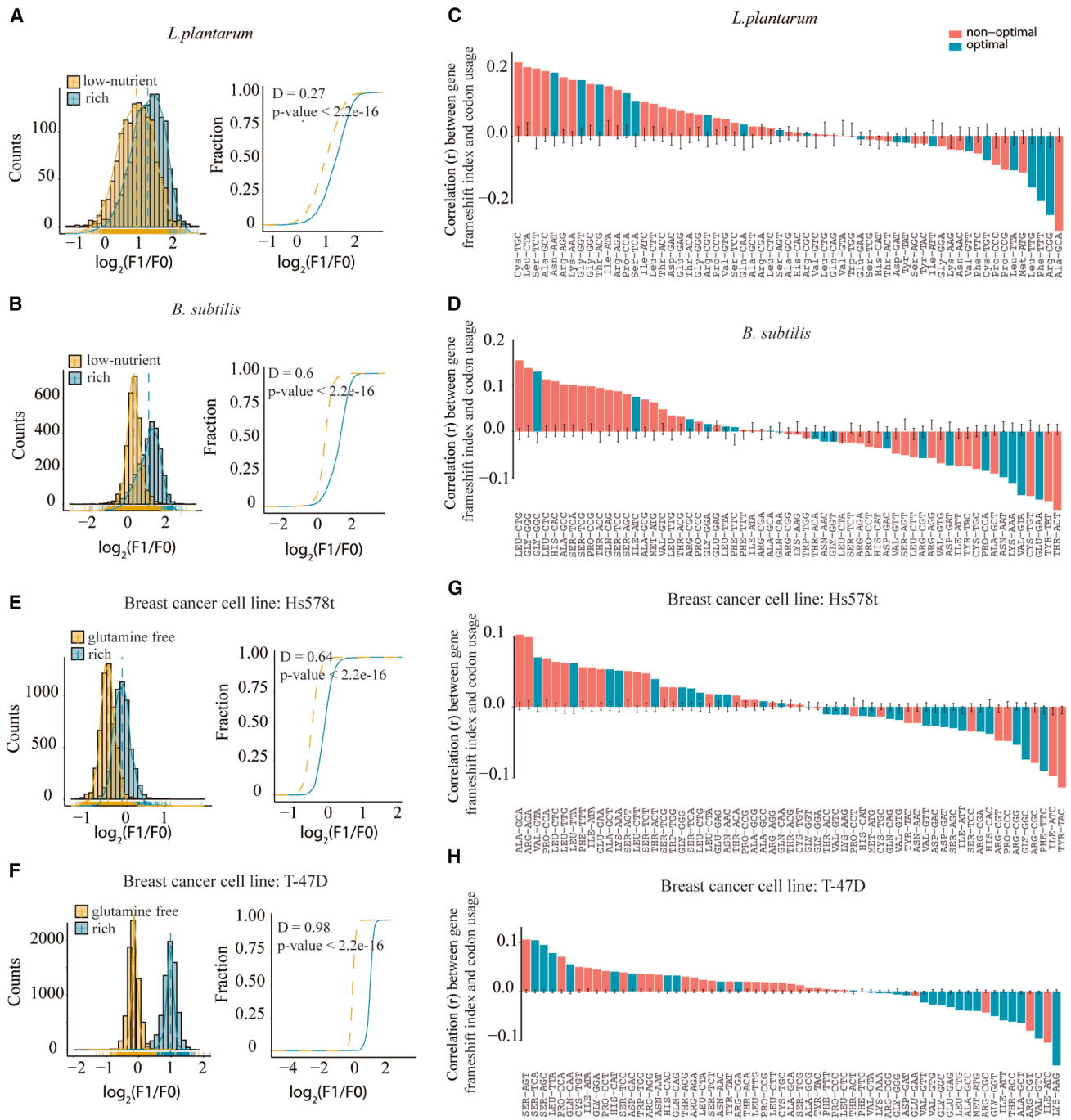


Figure 6. Nutrition-induced frameshifts are evolutionarily conserved from bacteria to human

(A) Distribution of gene-specific frameshift index for *L. plantarum* growing in rich (MRS broth) and after transferring it to low-nutrient conditions (0.5 × LB media) for 15 min (data obtained from Huch et al.⁹). A cumulative fraction plot with the frameshift index distribution is shown on the right. Statistical analysis is performed using a Kolmogorov-Smirnov test with p value and D as the distance between control and treatment distributions.

(B) Same as (A), but for *B. subtilis* exponentially growing in rich media (LB) and in low-nutrient conditions (minimal growth medium) (see STAR Methods section). (C) Pearson correlation between gene-specific frameshift index and codon usage. Only genes ($\log_2(F1/F0)_{\text{control}} > 0$ and $\log_2(F1/F0)_{\text{treatment}} < 0$) in *L. plantarum* were used for calculating correlations. Codons defined as optimal (in green) or non-optimal (in red) codons according to codon adaptation index obtained from Fuglsang.⁴¹

(D) Same as (C), but for *B. subtilis*. tRNA adaptation index was obtained from Perach et al.⁴²

(legend continued on next page)

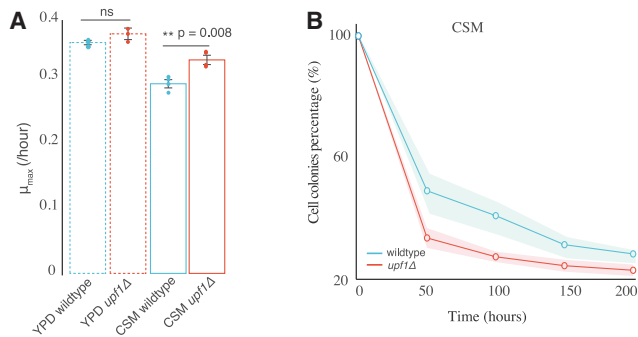


Figure 7. NMD limits cell proliferation in low-nutrient condition
(A) Maximum growth rates estimated from growth curve in wild-type (BY4741) and NMD mutant (*upf1Δ*) both in YPD and CSM. Statistical analysis was performed using two-sided t tests. ** $p = 0.008$.
(B) Cell viability after stationary phase in CSM. Cells were grown in CSM for 3 days to reach stationary phase (day 3, time 0). Samples were then collected every 48 h and plated for colony counting ($n = 3$ biological replicates).

versa (Figures 6C, 6D, S6B, and S6C; Table S6). This analysis demonstrates that also in prokaryotes, mRNAs more prone to displaying environmentally regulated frameshifts are enriched in non-optimal codons.

Lastly, we expanded our analysis to explore whether low-nutrient conditions induce generalized ribosome frameshifting in human cells (Figures 6E–6H). We reanalyzed ribosome profiling data from basal and luminal breast cancer cell lines after 48 h growth in glutamine-free medium.⁴³ All analyzed cell lines exhibited a significant increase in *out-of-frame* ribosome protection patterns (Figure S6D). This was particularly clear for Hs578t (frameshift transcripts increased from 3,237 to 5,222 transcripts, from 61.4% to 99% of detected transcripts) and T-47D (frameshift transcripts increased from 13 to 5,830, from 0.1% to 83% of detected transcripts) (Figures 6E, 6F, and S6E). Although *out-of-frame* ribosome protection appears to dominate at the RNA level, a significant portion of each mRNA may still undergo canonical translation, potentially supporting the slow growth observed in glutamine-free conditions. Overall, our findings show that environmentally induced ribosome frameshifting is a conserved process from bacteria to humans.

NMD limits cellular growth in low-nutrient conditions

Having observed that accelerated global mRNA decay via ribosome frameshifting in response to low-nutrient conditions is general in biology, we wondered in which conditions this would be advantageous for the cells. Our data suggest that cells can repurpose the NMD degradation machinery to limit mRNA abundance. We hypothesize that this should also restrict translation and thus cell growth. To test this, we first compared the maximum growth rate of exponentially growing cells with (wild type) and without active NMD (*upf1Δ*) (Figure 7A; Table S7). The *upf1Δ* strain

showed significantly increased growth rates compared with wild type in CSM media, suggesting that NMD plays a crucial role in restraining cell growth under nutrition limitation. Restricting cell growth and conserving limiting resources during nutrient deprivation is reminiscent of the bacterial stringent response that allows cells to survive the metabolic stress and enter a dormancy state in a reversible way.⁴⁵ We hypothesized that growth limitation caused by NMD-dependent mRNA decay could facilitate the adaptation of eukaryotic cells to nutrient-limited conditions by promoting entry into a quiescent state, thereby potentially enhancing cell survival during stress. To test this hypothesis, we assessed cell viability after prolonged starvation. We cultured cells to stationary phase and monitored cell viability over 8 days (Figure 7B; Table S7). Consistent with our hypothesis, wild-type cells exhibited higher viability compared with *upf1Δ*. We propose that this observed phenotype represents an adaptive strategy whereby wild-type cells conserve energy and resources by slowing down cell division in unfavorable environments.

DISCUSSION

Quality control pathways are essential to ensure that aberrant mRNAs or proteins are cleared out from the cells. In general, quality control mechanisms are energetically expensive. Thus, checkpoint mechanisms are in place to ensure that they only act on aberrant molecules. Here, we have shown that mRNA quality control is repurposed to globally control mRNA stability during poor nutrient conditions. Our work shows that ribosomes induce massive genome-wide frameshift events by sensing limiting nutritional conditions. We hypothesize that this could be a mechanism for ribosomes to easily control mRNA life by facilitating its decay. Here, we have examined the position of ribosomes associated with mRNA decay and identified that about 77% of the *S. cerevisiae* transcriptome is undergoing -1 frameshift-associated decay under low-nutrition conditions. Although this phenomenon is obvious in poor media, a small fraction of genes also shows preferential *out-of-frame* 5'P degradation signatures in optimal growth conditions. This suggests that *out-of-frame* decay plays a central role in gene expression and that, despite the known ability of NMD to target canonical mRNAs,^{14–16} the magnitude of its effect has likely been underestimated. We suspect that it is due to the fact that previous work focused mainly on the bulk of translating ribosomes and ignored the subset of mRNAs undergoing degradation that are transient and difficult to study. Importantly, this environmentally induced *out-of-frame* decay was also evident when investigating the mRNA turnover using RNA metabolic labeling. Using SLAM-seq,³⁰ we estimated that NMD-associated decay accounts for a minimum of 32% of the total decay rate in low-nutrition conditions.

To understand how ribosomes induce genome-wide -1 frameshifts in poor nutritional conditions, we investigated the potential involvement of known PRF sites. -1 PRF is often

(E) Same as (A), but for cell line Hs578t growing in rich media (DMEM medium) and in glutamine-deprived conditions. Data obtained from Loayza-Puch et al.⁴³
(F) Same as (A), but for cell line T-47D.
(G) Same as (C), but for Hs578t. Optimal codons and non-optimal codons are shown in green and red, respectively, according to Forrest et al.⁴⁴
(H) Same as (G), but for cell line T-47D.

associated with the presence of a heptanucleotide slippery sequence (X XXY YYZ) and a downstream secondary structure element.⁴⁶ The slippery sequence promotes ribosome slippage into the alternative frame, enabling codon-anticodon interactions in both frames, while the secondary structure element serves to slow down the ribosome at that position. The more optimistic estimates suggest that PRF sites exist in around 10% of all protein-coding genes across organisms.^{21,22} However, our work indicates that in our experimental conditions, the bulk of the transcriptome experiences a frameshift independent of known PRF sites (Figure S4; Table S4).

On the contrary, we highlight the role of low codon optimality in the appearance of environmentally induced ribosome frameshifts. This suggests that the molecular mechanism underlying the massive frameshifts that we report here could be related to the hungry codon frameshifts that occur during ribosome translocation via tRNA slippage of the P-site while the A-site is vacant.^{19,36,37} This frameshift mechanism can be coupled⁴⁷ or be independent³⁶ of *cis* elements, enhancing its efficiency (i.e., secondary structure elements), and is conserved from bacteria to mammals. Recent work has demonstrated that lower concentrations of charged tRNA^{Gln-CUG} enhance frameshifts associated with the CAG-encoded polyglutamine repeats in huntingtin (Htt).⁴⁸ Similarly, it has been shown in mouse embryonic fibroblasts that amino acid deprivation can lead to selective uncharging of glutamine-specific tRNAs and an increase of frameshifts in proteins containing polyglutamine tracks.⁴⁹ While previous studies focus on particular genes or tRNAs, our work demonstrates how a similar phenomenon can rewire gene expression by affecting the bulk of the transcriptome.

The model for environmentally induced frameshifts that we propose here suggests that the action of NMD will be key to regulating mRNA stability in those conditions (Figure 1D). Interestingly, NMD has been previously shown to preferentially target transcripts with lower codon optimality.²⁸ In fact, Celik et al. showed that NMD substrates tend to have a significantly higher ratio of *out-of-frame* reads as measured by ribosome profiling, something that further supports our working model. Here, we show that NMD targeting through ribosome frameshifting is modulated by nutritional conditions. Although we describe a nutrition-induced frameshift mechanism, our work supports a general strategy in which NMD can be used to regulate mRNA abundance, as previously proposed by the Dinman lab.⁵⁰ Furthermore, we show that the correlation between low codon optimality and frameshift-associated decay is maintained in bacteria that lack canonical NMD.⁵¹ This suggests that not only NMD but also general mRNA degradation and quality control mechanisms are used to transfer environmental information into mRNA decay signatures via ribosome frameshifting in both eukaryotes and prokaryotes. Interestingly, the mechanism that we report here is different from the previously reported role of ribosome collisions in signal transduction.⁵² In fact, in our conditions, we do not observe an increase but rather a decrease of disomes (Figure S1D). We hypothesize that, when low-nutrition conditions are maintained over time, both translation initiation and elongation are limited (Figures S1D and S1E). This would reduce the likelihood of ribosome collisions but not affect the frameshift-mediated mechanism that we propose here.

In addition to mRNA degradation, the massive frameshifting we describe can be expected to affect the proteome. Decreasing the abundance of available mRNA templates for translation directly affects protein synthesis. As expected, we observe that genes with a higher level of frameshifts present a lower relative protein abundance than those with lower frameshifts (Figure 5C). Furthermore, using a reporter system, we show that this mechanism leads to a dramatic decrease in ribosome efficiency, where less than 50% of the translation events lead to a full protein synthesis (Figure 4G). Our observations are congruent with previous work investigating alternative mRNA quality control pathways. For example, it has previously been demonstrated that ribosome stalling at non-optimal codons can reduce protein synthesis rates by increasing mRNA decay rates via NGD.¹¹ As we observe a decrease in ribosome collisions during continued growth in low nutrients (Figures S1D and S1E), our work suggests that frameshifts and not only ribosome collisions can transduce nutritional information into gene expression regulation. The regulation of protein abundance via frameshifting and increased mRNA decay further supports the role of ribosomes as nutritional sensors for dynamic regulation of a functional and balanced proteome. Our data showing that NMD can restrict cellular growth in low-nutrient conditions suggest that in eukaryotes, nutritional sensing by ribosomes followed by NMD decay could exert a function similar to the stringent response in bacteria. Namely, allowing cells to conserve limiting resources during nutrient deprivation, survive the metabolic stress, and enter a dormancy state in a reversible way.⁴⁵

Altogether, our work suggests that the translation process can act as a sensor for the dynamic regulation of a functional and balanced proteome by directly regulating mRNA life. Increased mRNA decay under poor nutritional conditions will limit energy used for translation. This raises the possibility that frameshifting may be beneficial for cells also in terms of releasing ribosomes and facilitating the degradation of peptides for subsequent recycling in response to low-nutrition conditions. Finally, faster mRNA turnover should also facilitate rewiring of the transcriptome and a swifter adaptation to new environments, something especially beneficial for unicellular organisms.

Limitations of the study

We have shown that environmentally induced frameshift is general in biology. Although our work demonstrates that the activation of NMD is a significant downstream consequence of these frameshifts, our results also highlight a complex interplay among various RNA degradation pathways, warranting further investigation. This is particularly important when considering that RNA degradation can be influenced by environmental changes.⁶ In addition to the general response regarding mRNA stability, frameshift events during translation elongation can be expected to generate aberrant proteins with canonical N-terminal polypeptide sequences and altered C-terminal regions.⁵³ Although those events are expected to be very rare, the presence of proteins with altered C-terminal regions could lead to the increase of protein aggregates or other proteostasis problems, as suggested by our reporter system. Additional research will be required to determine the potential impact on cell physiology of the putatively generated frameshifted peptides. Our work

also proposes a model where NMD limits cell growth in low-nutrition conditions. This raises the appealing possibility that ribosome frameshifting followed by NMD decay could facilitate the entry into quiescence for eukaryotic cells. We hypothesize that in eukaryotes, NMD could exert an analogous function to the type II RelE/RelB toxin-antitoxin system in bacteria that leads to a generalized mRNA degradation in response to low-nutrition conditions.^{54,55} This mechanism could be relevant to understanding how eukaryotic cells could escape antifungal treatment or even chemotherapy. However, additional work would be required to explore this hypothesis.

RESOURCE AVAILABILITY

Lead contact

Further information and requests for resources and reagents should be directed to and will be fulfilled by the lead contact, Vicent Pelechano (vicente.pelechano.garcia@ki.se).

Materials availability

This study did not generate new, unique materials or reagents.

Data and code availability

- The raw and processed sequencing data in this study (HT-5PSeq, SLAM-seq, and Ribo-seq) are deposited in GEO with accession numbers GEO: GSE230202, GSE230203, and GSE230204. The mass spectrometry proteomics data have been deposited to the ProteomeXchange Consortium via the PRIDE partner repository with the dataset identifier PRIDE: PXD042854. These data are publicly available as of the date of publication.
- This paper does not report original code.
- Any additional information required to reanalyze the data reported in this paper is available from the [lead contact](#) upon request.

ACKNOWLEDGMENTS

We thank all members of the Pelechano, Kutter, and Friedländer laboratories for useful discussions and suggestions. We thank José E. Pérez Ortín for additional feedback. Computational analysis was performed on resources provided by SNIC through Uppsala Multidisciplinary Center for Advanced Computational Science. This project was funded by the Swedish Foundation's Starting Grant (Ragnar Söderberg Foundation), a European Research Council (ERC) synergy grant EPIC 101118521, a Wallenberg Academy Fellowship (2016.0123 and 2021.0167), the Swedish Research Council (VR 2016-01842, 2020-01480, 2019-02335, and 2024-03210), the Karolinska Institutet (SciLifeLab Fellowship, SFO and KI funds), a Joint China-Sweden mobility grant (STINT, CH2018-7750), and a Humboldt Research Fellowship for Experienced Researchers (SWE 1221518 HFST-E) to V.P. Y.Z. was funded by a fellowship from the China Scholarship Council. L.N. acknowledges funding from the EU H2020-MSCA-IF-2018 program under grant agreement (845495 - TERMINATOR) and SC RA grant agreement (21SCG-1F006). I.P. receives funding from the Helmholtz Young Investigators program of the Helmholtz Association and from the European Research Council (ERC) under the European Union's Horizon 2020 research and innovation program (grant agreement ERC-STG no. 948544). P.S. is the recipient of grants from the Swedish Cancer Fund (19-0133 and 22-2014).

AUTHOR CONTRIBUTIONS

V.P., Y.Z., and L.N. conceived the project. Y.Z. performed most of the experimental and computational work. L.N. contributed to the frameshift analysis and discussion. E.F. performed the proteomic analysis under the supervision of I.P. C.B. contributed to proteomic data analysis. I.A. provided additional experimental assistance. C.S. contributed to frameshift reporters and revision.

S.H. contributed to polysome isolation and discussion. E.G. and P.S. contributed to initial experiments and discussion. Y.Z. and V.P. drafted the original manuscript. All authors reviewed and edited the manuscript. V.P. supervised the project.

DECLARATION OF INTERESTS

V.P., S.H., and L.N. are co-founders and shareholders of 3N Bio AB, which has filed a patent application regarding the study of the microbial degradome.

STAR★METHODS

Detailed methods are provided in the online version of this paper and include the following:

- **KEY RESOURCES TABLE**
- **EXPERIMENTAL MODEL AND STUDY PARTICIPANT DETAILS**
 - Strains and growth conditions
- **METHOD DETAILS**
 - HT-5Pseq library preparation
 - HT-5Pseq data processing and analysis
 - SLAM-seq metabolic labeling
 - SLAM-seq data analysis
 - Ribosome profiling library preparation
 - Ribosome profiling data analysis
 - Dual-fluorescent frameshifting assays
 - Sample preparation for proteomics analysis
 - Cell lysis and protein extraction for proteomics analysis
 - In-solution protein digestion for proteomics analysis
 - Liquid chromatography-mass spectrometry for proteomics analysis
 - Quantitative proteomics data analysis
- **QUANTIFICATION AND STATISTICAL ANALYSIS**

SUPPLEMENTAL INFORMATION

Supplemental information can be found online at <https://doi.org/10.1016/j.molcel.2025.04.022>.

Received: February 14, 2024

Revised: December 17, 2024

Accepted: April 16, 2025

Published: May 15, 2025

REFERENCES

- Houseley, J., and Tollervey, D. (2009). The Many Pathways of RNA Degradation. *Cell* 136, 763–776. <https://doi.org/10.1016/j.cell.2009.01.019>.
- Johnson, J.L., Stoica, L., Liu, Y., Zhu, P.J., Bhattacharya, A., Buffington, S. A., Huq, R., Eissa, N.T., Larsson, O., Porse, B.T., et al. (2019). Inhibition of Upf2-Dependent Nonsense-Mediated Decay Leads to Behavioral and Neurophysiological Abnormalities by Activating the Immune Response. *Neuron* 104, 665–679.e8. <https://doi.org/10.1016/j.neuron.2019.08.027>.
- Garcia-Moreno, M., Noerenberg, M., Ni, S., Järvelin, A.I., González-Almela, E., Lenz, C.E., Bach-Pages, M., Cox, V., Avolio, R., Davis, T., et al. (2019). System-wide Profiling of RNA-Binding Proteins Uncovers Key Regulators of Virus Infection. *Mol. Cell* 74, 196–211.e11. <https://doi.org/10.1016/j.molcel.2019.01.017>.
- Olivas, W., and Parker, R. (2000). The Puf3 protein is a transcript-specific regulator of mRNA degradation in yeast. *EMBO J.* 19, 6602–6611. <https://doi.org/10.1093/emboj/19.23.6602>.
- Sato, H., and Singer, R.H. (2021). Cellular variability of nonsense-mediated mRNA decay. *Nat. Commun.* 12, 7203. <https://doi.org/10.1038/s41467-021-27423-0>.
- Li, B., Zeis, P., Zhang, Y., Alekseenko, A., Fürst, E., Sanchez, Y.P., Lin, G., Tekkedil, M.M., Piazza, I., Steinmetz, L.M., et al. (2023). Differential

- regulation of mRNA stability modulates transcriptional memory and facilitates environmental adaptation. *Nat. Commun.* **14**, 910. <https://doi.org/10.1038/s41467-023-36586-x>.
7. Hu, W., Sweet, T.J., Chamnongpol, S., Baker, K.E., and Collier, J. (2009). Co-translational mRNA decay in *Saccharomyces cerevisiae*. *Nature* **461**, 225–229. <https://doi.org/10.1038/nature08265>.
 8. Pelechano, V., Wei, W., and Steinmetz, L.M. (2015). Widespread co-translational RNA decay reveals ribosome dynamics. *Cell* **161**, 1400–1412. <https://doi.org/10.1016/j.cell.2015.05.008>.
 9. Huch, S., Nersisyan, L., Ropat, M., Barrett, D., Wu, M., Wang, J., Valeriano, V.D., Vardazaryan, N., Huerta-Cepas, J., Wei, W., et al. (2023). Atlas of mRNA translation and decay for bacteria. *Nat. Microbiol.* **8**, 1123–1136. <https://doi.org/10.1038/s41564-023-01393-z>.
 10. Presnyak, V., Alhusaini, N., Chen, Y.H., Martin, S., Morris, N., Kline, N., Olson, S., Weinberg, D., Baker, K.E., Graveley, B.R., et al. (2015). Codon optimality is a major determinant of mRNA stability. *Cell* **160**, 1111–1124. <https://doi.org/10.1016/j.cell.2015.02.029>.
 11. Simms, C.L., Yan, L.L., and Zaher, H.S. (2017). Ribosome Collision Is Critical for Quality Control during No-Go Decay. *Mol. Cell* **68**, 361–373. e5. <https://doi.org/10.1016/j.molcel.2017.08.019>.
 12. D'Orazio, K.N., and Green, R. (2021). Ribosome states signal RNA quality control. *Mol. Cell* **81**, 1372–1383. <https://doi.org/10.1016/j.molcel.2021.02.022>.
 13. Buschauer, R., Matsuo, Y., Sugiyama, T., Chen, Y.H., Alhusaini, N., Sweet, T., Ikeuchi, K., Cheng, J., Matsuki, Y., Nobuta, R., et al. (2020). The Ccr4-Not complex monitors the translating ribosome for codon optimality. *Science* **368**, eaay6912. <https://doi.org/10.1126/science.aay6912>.
 14. Lykke-Andersen, S., and Jensen, T.H. (2015). Nonsense-mediated mRNA decay: An intricate machinery that shapes transcriptomes. *Nat. Rev. Mol. Cell Biol.* **16**, 665–677. <https://doi.org/10.1038/nrm4063>.
 15. Kervestin, S., and Jacobson, A. (2012). NMD: A multifaceted response to premature translational termination. *Nat. Rev. Mol. Cell Biol.* **13**, 700–712. <https://doi.org/10.1038/nrm3454>.
 16. Karousis, E.D., and Mühlemann, O. (2022). The broader sense of nonsense. *Trends Biochem. Sci.* **47**, 921–935. <https://doi.org/10.1016/j.tibs.2022.06.003>.
 17. Nickless, A., Ballis, J.M., and You, Z. (2017). Control of gene expression through the nonsense-mediated RNA decay pathway. *Cell Biosci.* **7**, 26. <https://doi.org/10.1186/s13578-017-0153-7>.
 18. Dever, T.E., Dinman, J.D., and Green, R. (2018). Translation elongation and recoding in eukaryotes. *Cold Spring Harb. Perspect. Biol.* **10**, a032649. <https://doi.org/10.1101/cshperspect.a032649>.
 19. Temperley, R., Richter, R., Dennerlein, S., Lightowers, R.N., and Chrzanowska-Lightowers, Z.M. (2010). Hungry codons promote frameshifting in human mitochondrial ribosomes. *Science* **327**, 301. <https://doi.org/10.1126/science.1180674>.
 20. Rodnina, M.V., Korniy, N., Klimova, M., Karki, P., Peng, B.Z., Senyushkina, T., Belardinelli, R., Maracci, C., Wohlgemuth, I., Samatova, E., et al. (2020). Translational recoding: canonical translation mechanisms reinterpreted. *Nucleic Acids Res.* **48**, 1056–1067. <https://doi.org/10.1093/nar/gkz783>.
 21. Jacobs, J.L., Belew, A.T., Rakauskaitė, R., and Dinman, J.D. (2007). Identification of functional, endogenous programmed -1 ribosomal frameshift signals in the genome of *Saccharomyces cerevisiae*. *Nucleic Acids Res.* **35**, 165–174. <https://doi.org/10.1093/nar/gki1033>.
 22. Belew, A.T., Hepler, N.L., Jacobs, J.L., and Dinman, J.D. (2008). PRFdb: a database of computationally predicted eukaryotic programmed -1 ribosomal frameshift signals. *BMC Genomics* **9**, 339. <https://doi.org/10.1186/1471-2164-9-339>.
 23. Nersisyan, L., Ropat, M., and Pelechano, V. (2020). Improved computational analysis of ribosome dynamics from 5'P degradome data using five-seq. *NAR Genom. Bioinform.* **2**, lqaa099. <https://doi.org/10.1093/nar/gab/lqaa099>.
 24. Zhang, Y., and Pelechano, V. (2021). High-throughput 5'P sequencing enables the study of degradation-associated ribosome stalls. *Cell Rep. Methods* **1**, 100001. <https://doi.org/10.1016/j.crmeth.2021.100001>.
 25. Rodríguez-Galán, O., García-Gómez, J.J., Rosado, I.V., Wei, W., Méndez-Godoy, A., Pillet, B., Alekseenko, A., Steinmetz, L.M., Pelechano, V., Kressler, D., et al. (2021). A functional connection between translation elongation and protein folding at the ribosome exit tunnel in *Saccharomyces cerevisiae*. *Nucleic Acids Res.* **49**, 206–220. <https://doi.org/10.1093/nar/gkaa1200>.
 26. Pelechano, V., and Alepuz, P. (2017). EIF5A facilitates translation termination globally and promotes the elongation of many non polyproline-specific tripeptide sequences. *Nucleic Acids Res.* **45**, 7326–7338. <https://doi.org/10.1093/nar/gkx479>.
 27. Simms, C.L., Yan, L.L., Qiu, J.K., and Zaher, H.S. (2019). Ribosome Collisions Result in +1 Frameshifting in the Absence of No-Go Decay. *Cell Rep.* **28**, 1679–1689.e4. <https://doi.org/10.1016/j.celrep.2019.07.046>.
 28. Celik, A., Baker, R., He, F., and Jacobson, A. (2017). High-resolution profiling of NMD targets in yeast reveals translational fidelity as a basis for substrate selection. *RNA* **23**, 735–748. <https://doi.org/10.1261/ma.060541.116>.
 29. Gasch, A.P., Spellman, P.T., Kao, C.M., Carmel-Harel, O., Eisen, M.B., Storz, G., Botstein, D., and Brown, P.O. (2000). Genomic Expression Programs in the Response of Yeast Cells to Environmental Changes. *Mol. Biol. Cell* **11**, 4241–4257. <https://doi.org/10.1091/mbc.11.12.4241>.
 30. Herzog, V.A., Reichhoff, B., Neumann, T., Rescheneder, P., Bhat, P., Burkard, T.R., Wlotzka, W., Von Haeseler, A., Zuber, J., and Ameres, S. L. (2017). Thiol-linked alkylation of RNA to assess expression dynamics. *Nat. Methods* **14**, 1198–1204. <https://doi.org/10.1038/nmeth.4435>.
 31. García-Martínez, J., Delgado-Ramos, L., Ayala, G., Pelechano, V., Medina, D.A., Carrasco, F., González, R., Andrés-León, E., Steinmetz, L., Warringer, J., et al. (2016). The cellular growth rate controls overall mRNA turnover, and modulates either transcription or degradation rates of particular gene regulons. *Nucleic Acids Res.* **44**, 3643–3658. <https://doi.org/10.1093/nar/gkv1512>.
 32. Heck, A.M., and Wilusz, J. (2018). The interplay between the RNA decay and translation machinery in eukaryotes. *Cold Spring Harb. Perspect. Biol.* **10**, a032839. <https://doi.org/10.1101/cshperspect.a032839>.
 33. Tomaz da Silva, P., Zhang, Y., Theodorakis, E., Martens, L.D., Yépez, V.A., Pelechano, V., and Gagneur, J. (2024). Cellular energy regulates mRNA degradation in a codon-specific manner. *Mol. Syst. Biol.* **20**, 506–520. <https://doi.org/10.1038/s44320-024-00026-9>.
 34. Jacks, T., Power, M.D., Masiarz, F.R., Luciw, P.A., Barr, P.J., and Varmus, H.E. (1988). Characterization of ribosomal frameshifting in HIV-1 gag-pol expression. *Nature* **331**, 280–283. <https://doi.org/10.1038/331280a0>.
 35. Wilson, W., Braddock, M., Adams, S.E., Rathjen, P.D., Kingsman, S.M., and Kingsman, A.J. (1988). HIV expression strategies: Ribosomal frameshifting is directed by a short sequence in both mammalian and yeast systems. *Cell* **55**, 1159–1169. [https://doi.org/10.1016/0092-8674\(88\)90260-7](https://doi.org/10.1016/0092-8674(88)90260-7).
 36. Caliskan, N., Wohlgemuth, I., Korniy, N., Pearson, M., Peske, F., and Rodnina, M.V. (2017). Conditional Switch between Frameshifting Regimes upon Translation of dnaX mRNA. *Mol. Cell* **66**, 558–567.e4. <https://doi.org/10.1016/j.molcel.2017.04.023>.
 37. Gallant, J.A., and Lindsley, D. (1992). Leftward ribosome frameshifting at a hungry codon. *J. Mol. Biol.* **223**, 31–40. [https://doi.org/10.1016/0022-2836\(92\)90713-t](https://doi.org/10.1016/0022-2836(92)90713-t).
 38. Harger, J.W., and Dinman, J.D. (2003). An in vivo dual-luciferase assay system for studying translational recoding in the yeast *Saccharomyces cerevisiae*. *RNA* **9**, 1019–1024. <https://doi.org/10.1261/ma.5930803>.
 39. Rakauskaitė, R., Liao, P.Y., Rhodin, M.H.J., Lee, K., and Dinman, J.D. (2011). A rapid, inexpensive yeast-based dual-fluorescence assay of

- programmed-1 ribosomal frameshifting for high-throughput screening. *Nucleic Acids Res.* 39, e97. <https://doi.org/10.1093/nar/gkr382>.
40. Darnell, A.M., Subramaniam, A.R., and O'Shea, E.K. (2018). Translational Control through Differential Ribosome Pausing during Amino Acid Limitation in Mammalian Cells. *Mol. Cell* 71, 229–243.e11. <https://doi.org/10.1016/j.molcel.2018.06.041>.
 41. Fuglsang, A. (2003). Lactic acid bacteria as prime candidates for codon optimization. *Biochem. Biophys. Res. Commun.* 312, 285–291. <https://doi.org/10.1016/j.bbrc.2003.10.120>.
 42. Perach, M., Zafrir, Z., Tuller, T., and Lewinson, O. (2021). Identification of conserved slow codons that are important for protein expression and function. *RNA Biol.* 18, 2296–2307. <https://doi.org/10.1080/15476286.2021.1901185>.
 43. Loayza-Puch, F., Rooijers, K., Buil, L.C.M., Zijlstra, J., Oude Vrielink, J.F., Lopes, R., Ugalde, A.P., Van Breugel, P., Hofland, I., Wesseling, J., et al. (2016). Tumour-specific proline vulnerability uncovered by differential ribosome codon reading. *Nature* 530, 490–494. <https://doi.org/10.1038/nature16982>.
 44. Forrest, M.E., Pinkard, O., Martin, S., Sweet, T.J., Hanson, G., and Collier, J. (2020). Codon and amino acid content are associated with mRNA stability in mammalian cells. *PLoS One* 15, e0228730. <https://doi.org/10.1371/journal.pone.0228730>.
 45. Haurlyuk, V., Atkinson, G.C., Murakami, K.S., Tenson, T., and Gerdes, K. (2015). Recent functional insights into the role of (p)ppGpp in bacterial physiology. *Nat. Rev. Microbiol.* 13, 298–309. <https://doi.org/10.1038/nrmicro3448>.
 46. Brierley, I., Digard, P., and Inglis, S.C. (1989). Characterization of an Efficient Coronavirus Ribosomal Frameshifting Signal: Requirement for an RNA Pseudoknot. *Cell* 57, 537–547. [https://doi.org/10.1016/0092-8674\(89\)90124-4](https://doi.org/10.1016/0092-8674(89)90124-4).
 47. Atkinson, J., Dodge, M., and Gallant, J. (1997). Secondary structures and starvation-induced frameshifting. *Mol. Microbiol.* 26, 747–753. <https://doi.org/10.1046/j.1365-2958.1997.6101959.x>.
 48. Girstmair, H., Saffert, P., Rode, S., Czech, A., Holland, G., Bannert, N., and Ignatova, Z. (2013). Depletion of Cognate Charged Transfer RNA Causes Translational Frameshifting within the Expanded CAG Stretch in Huntingtin. *Cell Rep.* 3, 148–159. <https://doi.org/10.1016/j.celrep.2012.12.019>.
 49. Pavlova, N.N., King, B., Josselson, R.H., Violante, S., Macera, V.L., Vardhana, S.A., Cross, J.R., and Thompson, C.B. (2020). Translation in amino-acid-poor environments is limited by tRNA^{Gln} charging. *eLife* 9, e62307. <https://doi.org/10.7554/eLife.62307>.
 50. Belew, A.T., Advani, V.M., and Dinman, J.D. (2011). Endogenous ribosomal frameshift signals operate as mRNA destabilizing elements through at least two molecular pathways in yeast. *Nucleic Acids Res.* 39, 2799–2808. <https://doi.org/10.1093/nar/gkq1220>.
 51. Belasco, J.G. (2010). All things must pass: contrasts and commonalities in eukaryotic and bacterial mRNA decay. *Nat. Rev. Mol. Cell Biol.* 11, 467–478. <https://doi.org/10.1038/nrm2917>.
 52. Wu, C.C.-C., Peterson, A., Zinshteyn, B., Regot, S., and Green, R. (2020). Ribosome Collisions Trigger General Stress Responses to Regulate Cell Fate. *Cell* 182, 404–416.e14. <https://doi.org/10.1016/j.cell.2020.06.006>.
 53. Bartok, O., Pataskar, A., Nagel, R., Laos, M., Goldfarb, E., Hayoun, D., Levy, R., Körner, P.R., Kreuger, I.Z.M., Champagne, J., et al. (2021). Anti-tumour immunity induces aberrant peptide presentation in melanoma. *Nature* 590, 332–337. <https://doi.org/10.1038/s41586-020-03054-1>.
 54. Page, R., and Peti, W. (2016). Toxin-antitoxin systems in bacterial growth arrest and persistence. *Nat. Chem. Biol.* 12, 208–214. <https://doi.org/10.1038/nchembio.2044>.
 55. Neubauer, C., Gao, Y.G., Andersen, K.R., Dunham, C.M., Kelley, A.C., Hentschel, J., Gerdes, K., Ramakrishnan, V., and Brodersen, D.E. (2009). The Structural Basis for mRNA Recognition and Cleavage by the Ribosome-Dependent Endonuclease RelE. *Cell* 139, 1084–1095. <https://doi.org/10.1016/j.cell.2009.11.015>.
 56. Smith, T., Heger, A., and Sudbery, I. (2017). UMI-tools: Modeling sequencing errors in Unique Molecular Identifiers to improve quantification accuracy. *Genome Res.* 27, 491–499. <https://doi.org/10.1101/gr.209601.116>.
 57. Dobin, A., Davis, C.A., Schlesinger, F., Drenkow, J., Zaleski, C., Jha, S., Batut, P., Chaisson, M., and Gingeras, T.R. (2013). STAR: Ultrafast universal RNA-seq aligner. *Bioinformatics* 29, 15–21. <https://doi.org/10.1093/bioinformatics/bts635>.
 58. Thorvaldsdóttir, H., Robinson, J.T., and Mesirov, J.P. (2013). Integrative Genomics Viewer (IGV): High-performance genomics data visualization and exploration. *Brief. Bioinform.* 14, 178–192. <https://doi.org/10.1093/bib/bbs017>.
 59. Zhou, Y., Zhou, B., Pache, L., Chang, M., Khodabakhshi, A.H., Tanaseichuk, O., Benner, C., and Chanda, S.K. (2019). Metascape provides a biologist-oriented resource for the analysis of systems-level datasets. *Nat. Commun.* 10, 1523. <https://doi.org/10.1038/s41467-019-09234-6>.
 60. Gu, Z., Eils, R., and Schlesner, M. (2016). Complex heatmaps reveal patterns and correlations in multidimensional genomic data. *Bioinformatics* 32, 2847–2849. <https://doi.org/10.1093/bioinformatics/btw313>.
 61. Yu, G., Wang, L.G., Han, Y., and He, Q.Y. (2012). ClusterProfiler: An R package for comparing biological themes among gene clusters. *Omic* 16, 284–287. <https://doi.org/10.1089/omi.2011.0118>.
 62. Carneiro, R.L., Requião, R.D., Rossetto, S., Domitrovic, T., and Palhano, F. L. (2019). Codon stabilization coefficient as a metric to gain insights into mRNA stability and codon bias and their relationships with translation. *Nucleic Acids Res.* 47, 2216–2228. <https://doi.org/10.1093/nar/gkz033>.
 63. Xu, Z., Wei, W., Gagneur, J., Perocchi, F., Clauder-Münster, S., Camblong, J., Guffanti, E., Stutz, F., Huber, W., and Steinmetz, L.M. (2009). Bidirectional promoters generate pervasive transcription in yeast. *Nature* 457, 1033–1037. <https://doi.org/10.1038/nature07728>.
 64. Pelechano, V., Wei, W., and Steinmetz, L.M. (2013). Extensive transcriptional heterogeneity revealed by isoform profiling. *Nature* 497, 127–131. <https://doi.org/10.1038/nature12121>.
 65. Latorre, P., Böttcher, R., Nadal-Ribelles, M., Li, C.H., Solé, C., Martínez-Cebrián, G., Boutros, P.C., Posas, F., and de Nadal, E. (2022). Data-driven identification of inherent features of eukaryotic stress-responsive genes. *NAR Genom Bioinform* 4, lqac018. <https://doi.org/10.1093/nargab/lqac018>.
 66. Voichek, Y., Bar-Ziv, R., and Barkai, N. (2016). Expression homeostasis during DNA replication. *Science* 351, 1087–1090.
 67. Chan, L.Y., Mugler, C.F., Heinrich, S., Vallotton, P., and Weis, K. (2018). Non-invasive measurement of mRNA decay reveals translation initiation as the major determinant of mRNA stability. *eLife* 7, e32536. <https://doi.org/10.7554/eLife.32536>.
 68. Gandin, V., Sikström, K., Alain, T., Morita, M., McLaughlan, S., Larsson, O., and Topisirovic, I. (2014). Polysome Fractionation and Analysis of Mammalian Translatomes on a Genome-wide Scale. *J. Vis. Exp.* 87, 51455. <https://doi.org/10.3791/51455>.

STAR★METHODS

KEY RESOURCES TABLE

REAGENT or RESOURCE	SOURCE	IDENTIFIER
Bacterial and virus strains		
<i>Bacillus subtilis</i> 168trpC2	Huch, et.al, ⁹	N/A
Chemicals, peptides, and recombinant proteins		
Acid-Phenol:Chloroform, pH 4.5 (with IAA, 125:24:1)	Thermo Fisher Scientific	AM9722
dNTP set, 100mM solution	Thermo Fisher Scientific	R0181
Phenol Solution. Saturated with 0.1M citrate buffer, pH 4.3 ± 0.2	Sigma-Aldrich	P4682
Chloroform:isoamyl alcohol 24:1	Sigma-Aldrich	C0549
Nuclease-free water, not DEPC treated	Thermo Fisher Scientific	AM9937
Ribolock RNase inhibitor 40 000U/mL	Thermo Fisher Scientific	EO0382
Glycoblue coprecipitant (15mg/mL)	Thermo Fisher Scientific	AM9515
T4 RNA ligase 1	NEB	M0204L
SuperScript™ II Reverse Transcriptase	Thermo Fisher Scientific	18064071
Phusion® High-Fidelity PCR Master Mix	NEB	M0531S
AMPure XP	Beckman Coulter	A63881
RNAClean XP	Beckman Coulter	A63987
Glass beads, acid-washed	Sigma-Aldrich	G8772
Sodium Acetate buffer solution, pH 5.3	Sigma-Aldrich	S7899
Duplex-specific nuclease	Evrogen	EA002
COMPLETE CSM MIXTURE	Formedium	DCS0019
SC-URA	MP Biomedicals	114410622-CF
SC-HIS	MP Biomedicals	114410222
Uracil	MP Biomedicals	02103204-CF
iron ammonium citrate	Fisher Scientific	0971350G
Tryptophan	Sigma	93659
Arginine	Sigma	A1270000
Proline	Sigma	81709
Serine	Sigma	84959
Alanine	Sigma	A7627
Histidine	Sigma	H0750000
Lysine	Sigma	L5501
Methionine	Sigma	64319
Leucine	Sigma	L8912
Asparagine	Sigma	A0884
RNase I	Ambion	AM2294
Superscript	Thermo Fisher	AM2696
15 % TBE-urea gel	Thermo Scientific	EC6885BOX
4-thiouracil	Sigma	440736
Cycloheximide	Sigma	C7698
MES	Sigma	M3671-50G
T4 PNK	NEB	M0201S
Superscript II	Fisher Scientific	18064071
Critical commercial assays		
Turbo Dnase kit	Thermo Fisher Scientific	AM1907

(Continued on next page)

Continued		
REAGENT or RESOURCE	SOURCE	IDENTIFIER
High-sensitivity DNA kit	Agilent	5067-4626
Qubit™ dsDNA HS Assay Kit	Thermo Fisher Scientific	Q32854
Qubit™ RNA HS assay kit	Thermo Fisher Scientific	Q32852
Qubit™ RNA Nano 6000 kit	Thermo Fisher Scientific	Q33221
RiboPools Depletion Kit	siTOOLs Biotech	N/A
Small RNA Sample Preparation Kit	NEXTFLEX	NOVA-5132-32
Ultra™ II Directional RNA Library Prep Kit	NEB	E7760S
Deposited data		
The raw and processed sequencing data for HT5Pseq	This study	GSE230202
The raw and processed sequencing data for SLAM-Seq	This study	GSE230204
The raw and processed sequencing data for Ribosome profiling	This study	GSE230203
Proteomics	This study	PXD042854
Experimental models: Organisms/strains		
<i>Saccharomyces cerevisiae</i> strains:BY4741:(MATa his3Δ1 leu2Δ0 met15Δ0 ura3Δ0)	NA	NA
<i>Saccharomyces cerevisiae</i> strains:upf1Δ(MATa his3Δ1 leu2Δ0 met15Δ0 ura3Δ0 upf1Δ)	NA	NA
<i>Saccharomyces cerevisiae</i> strains: DCP2-7::KanR; his31 leu20 ura30 met150	NA	NA
<i>Saccharomyces cerevisiae</i> strains: dhh1Δ(MATa his3Δ1 leu2Δ0 met15Δ0 ura3Δ0 dhh1Δ)	NA	NA
<i>Saccharomyces cerevisiae</i> strains: gcn1Δ(MATa his3Δ1 leu2Δ0 met15Δ0 ura3Δ0 gcn1Δ)	NA	NA
<i>Saccharomyces cerevisiae</i> strains: gcn1Δupf1Δ(MATa his3Δ1 leu2Δ0 met15Δ0 ura3Δ0 gcn1Δupf1Δ)	This study	NA
<i>Saccharomyces cerevisiae</i> strains: BY4741:: p416TEF-RFP-PRF-GFP (see Table S4)	This study	NA
<i>Saccharomyces cerevisiae</i> strains: BY4741:: p416TEF-RFP-mutated_PRF-GFP(see Table S4)	This study	NA
<i>Saccharomyces cerevisiae</i> strains: BY4741:: p416TEF-RFP-6xProline-GFP(see Table S4)	This study	N/A
<i>Saccharomyces cerevisiae</i> strains: BY4741:: p416TEF-RFP-6x Arginine-GFP(see Table S4)	This study	N/A
Oligonucleotides		
Primer for frameshift reporter, see Table S4	This study	N/A
Recombinant DNA		
Plasmid: p416TEF	Li et al. ⁶	N/A
Software and algorithms		
Fivepseq package 1.2.0	Nersisyan et al. ²³	https://github.com/lilit-nersisyan/fivepseq
bcl2fastq v2.20.0	Illumina	https://emea.support.illumina.com/sequencing/sequencing_software/bcl2fastq-conversion-software.html
Cutadapt v1.16	GitHub	https://github.com/marcelm/cutadapt/
UMI-tools	Smith et al. ⁵⁶	https://github.com/CGATOxford/UMI-tools
STAR v2.7.0	Dobin et al. ⁵⁷	https://github.com/alexdobin/STAR
IGV	Thorvaldsdóttir et al. ⁵⁸	https://igv.org
RStudio v4.0.4	RStudio, Inc., Boston, MA	N/A
slamdunk v0.4.3	nfcore pipeline	https://nf-co.re/slamsseq
riboSeqR	RStudio, Inc., Boston, MA	N/A
metascape v3.5	Zhou et al. ⁵⁹	https://metascape.org/gp/index.html#/main/step1

EXPERIMENTAL MODEL AND STUDY PARTICIPANT DETAILS

Strains and growth conditions

All yeast experiments were performed using *Saccharomyces cerevisiae* strain BY4741 (MATa *his3Δ1 leu2Δ0 met15Δ0 ura3Δ0*) if not stated otherwise. *S. cerevisiae* was grown to mid exponential phase ($OD_{600} \sim 0.6$) at 30 °C with rotation using YPD (1% yeast extract, 2% peptone, 2% glucose), Complete Supplement Mixture (CSM from Formedium™) or Synthetic Complete (SC from MP Biomedicals™) medium (composition details seen in Table S1). For bacteria, *B. subtilis* (168 *trpC2*) was collected after reaching the mid-exponential phase ($OD_{600} \sim 0.6$) in LB or in Minimal growth medium.

METHOD DETAILS

To measure the growth curve, cells were initially pre-cultivated at 30°C with rotation overnight until reaching the mid-exponential phase ($OD_{600} \sim 0.6$). Subsequently, the cells were diluted to an OD_{600} of approximately 0.01 in preparation for measurement using a plate reader. OD_{600} was measured every 10 minutes with 5 minutes of pre-shaking before each measurement. This process continued for a total duration of 40 hours.

Bacillus subtilis 168 (*trpC2*) strain was pre-cultivated at 37°C with rotation in LB and minimal growth medium (per 50 ml: 5X minimal salts solution, 10 ml; glucose (50% (w/v)), 0.5 ml; casamino acids (2% (w/v)), 0.5 ml; tryptophan (10 mg/ml), 0.1 ml; iron ammonium citrate (2.2 mg/ml), 0.05 ml, deionized water, 39 ml) with tryptophan supplementation at $OD_{600} < 0.8$. Cultures were diluted to $OD_{600} \sim 0.05$ and collected until reaching the mid-exponential phase ($OD_{600} \sim 0.6$).

For stress treatments in *S. cerevisiae*, we grew the cells to exponential phase, then split them into different flasks for different stress treatments. For heat shock, cells were exposed to 42°C for 30 minutes. For oxidative stress, cells were treated with 0.2 mM H_2O_2 for either 5 or 30 minutes. To induce amino acid deprivation, cells were quickly collected by centrifugation and then washed with CSM medium lacking amino acids. The cells were then incubated for 30 minutes (starting from the time they were first exposed to the amino acid deprived CSM medium). For glucose deprivation, mid exponential *S. cerevisiae* cultures at $OD_{600} \sim 0.8$ were spun down, washed twice, and resuspended in pre-warmed YP (lacking glucose) and then grown at 30°C for 5 minutes and 15 minutes as time points. To induce ribosome collisions in *S. cerevisiae*, we grew the cells to exponential phase in SC medium and then transfer them to SC media without histidine medium for 30 minutes. For addition of single amino acid experiment, arginine, proline, or serine were individually added as single amino acids to reach the comparable concentration as present in SC medium. Specifically, we increased the concentration of each amino acid from 50 to 85.6 mg/L for arginine, and from 0 to 85.6 mg/L in the case of proline and serine. *S. cerevisiae* was inoculated into each medium overnight as precultures. Cultures were diluted to $OD_{600} \sim 0.05$ and collected until reaching the mid-exponential phase ($OD_{600} \sim 0.6$) at 30°C.

All yeast and bacteria samples prepared for HT-5Pseq libraries were collected through centrifugation and preserved by freezing them in liquid nitrogen. Total RNA was isolated by the standard phenol: chloroform method and DNA was removed by DNase I treatment. RNA concentration was measured with Qubit and RNA quality was checked by 1.2% agarose gel or on a BioAnalyzer using an RNA Nano 6000 chip (Agilent Technologies).

For cell viability analysis after stationary phase in CSM, cells were grown in CSM medium for 3 days to reach stationary phase (designated as time 0). Samples were collected every 48 hours and plated on CSM agar plates for colony counting. Cell viability was quantified as colony-forming units per milliliter (CFU/mL).

HT-5Pseq library preparation

HT-5Pseq libraries were prepared following a previously established protocol²⁴ if not stated otherwise. Briefly, 6 μg of total RNA was subjected to DNase treatment, and the resulting DNA-free total RNA was ligated with an RNA oligo containing UMI (rP5_RND oligo). The ligated RNA was reverse transcribed using Illumina PE2 compatible oligos with random hexamers and oligo-dT as primers. To eliminate RNA in RNA/DNA hybrids, samples were treated with sodium hydroxide at 65°C for 20 minutes. Ribosomal RNAs were depleted using DSN (Duplex-specific nuclease) and a mixture of ribosomal DNA probes. To deplete Ribosomal RNAs in *B. subtilis* 168 (*trpC2*), we used the in-house rRNA DNA oligo depletion mixes described previously.⁹ Finally, the samples were amplified by PCR and sequenced on an Illumina NextSeq 2000 instrument using an average of 45 cycles for read1.

HT-5Pseq data processing and analysis

HT-5Pseq reads were demultiplexed using *bcl2fastq* (v2) and the 3' sequencing adapter was trimmed using *cutadapt* V4.0. After that, the 8-nt random barcodes located on the 5' ends of reads were extracted and added to the fastq file header as UMIs using *UMI-tools*⁵⁶. Reads were mapped to the reference genome (SGD R64-1-1 for *S. cerevisiae* and GCF_000009045.1_ASM904v1 for *B. subtilis*) using *star/2.7.0*⁶⁰ with the parameter `-alignEndsType Extend5pOfRead1` to exclude soft-clipped bases on the 5' end. Duplicated 5' ends of read introduced by PCR during library preparation were removed based on random barcodes sequences using *UMI-tools*. Analysis of 5' end positions was performed using the *fivepseq* package²³ version 1.2.0. This included analysis of the relative positions of the 5' ends of the mRNA reads with respect to the start codon, stop codon, and codon-specific pausing. Specifically, the unique 5' mRNA reads in biological samples were averaged and normalized to reads per million (rpm). The relative position of 5' mRNA reads at each codon were summed up and used for all additional analyses. Metagene plots for frame (F0, F1 or F2)

preference are shown as the average sum (in rpm) of each frame over a sliding window of 20 codons, for +/- 100 bp from the start and end, and for +/- 300 bp from the middle of CDS for each gene. *Fivepseq* output files will be deposited at the SciLifeLab Data repository. Genomic tracts from BAM files were visualized using IGV.⁵⁸

To calculate gene-specific frameshift index, we summed the reads for each frame of every transcript after excluding the first and last 50 nt. Transcripts with greater than 20 reads per million (rpm) were considered for subsequent analysis in each biological replicate. The frameshift index of each transcript was determined by dividing the number of in-frame reads (F1) by out-of-frame reads (F0), with the result expressed in logarithmic scale. Only transcripts that were present in all biological replicates were included in the calculation of frameshift index. Similarly, the frameshift index for each codon was calculated by dividing the in-frame reads at position -17 (F1) by the out-of-frame reads at position -18 (F0), with the result expressed in logarithmic scale. High frameshift genes are defined as: $\log_2(F1/F0)_{YPD} > 0.2$ and $\log_2(F1/F0)_{CSM} < -0.2$ (according to mean value in each distribution) and non-frameshift genes are defined as: $\log_2(F1/F0)_{YPD, CSM} > 0$.

Disomes were detected by the *fivepseq* package²³ in the queue statistics output using default parameters. For each gene, *fivepseq* first determines windows of periodicity 30 nt +/- 3.6 nt that have a Fast Fourier transform (FFT) signal of more than 20. The identified windows are then continuously extended and/or merged to bigger windows until the periodicity signal is no longer increasing. The merged windows are then sliced to a range between the two tallest peaks. Those peaks are determined based on the p value of a count falling within a Poisson distribution with a lambda corresponding to the average count in the given range. Counts with a p value less than 0.001 are considered peaks. In the context of FFT signals, a periodicity of 30 nt \pm 3.6 nt indicates the occurrence of two collided ribosomes (disomes). This periodicity indicates the presence of 2 adjacent protection sites separated exactly 30 nt (that is the distance covered by a full ribosome). Similarly, a length of 60 nt \pm 3.6 nt corresponds to the presence of three ribosomes, and this pattern continues for subsequent lengths.

To determine the proportion of the transcriptome degraded through *out-of-frame* co-translational decay in CSM, we used a simulation in which we mixed the codon protection index,⁸ defined as $\log_2(F1/((F2+F0)/2))$ from two samples at different ratios. Specifically, we combined the in-frame decay data from YPD (assuming a 100% of in-frame degradation) with simulated *out-of-frame* decay data (by shifting the YPD data by -1nt to generate a theoretical 100% *out-of-frame* decay). The use of the codon protection index instead of the frameshift index in this context is based on the fact that the YPD data shifted by -1nt, resulting in a change in all frames to the new corresponding -1nt frames. By using the codon protection index, we ensure that all frame changes are taken into consideration and properly accounted for in the analysis. We mixed both samples at different ratios (increasing 10% *out-of-frame* decay at each mixing) to estimate the median of each codon protection index distribution. Each mixing process was iterated 1000 times to obtain 95% confidence intervals. Finally, we used the generated distribution of codon protection indexes to estimate the percentage of *out-of-frame* co-translational decay.

To analyse whether the frameshift is induced by the programmed ribosomal frameshift slippery motif, we utilized putative PRF sites downloaded from PRFdb²² (Data S4). 5PSeq reads were aligned to the annotated slippery sequences motifs with an extension of 99 bp both upstream and downstream. We calculated the coverage for each frame by applying a sliding window of 3 nucleotides and taking the average. Finally, we plotted the calculated proportion for each frame.

To analyse frameshift in *B. subtilis* 168 trpC2 at early stationary phase and *L. plantarum* in low nutrients, we obtained the dataset from Huch et al.⁹ with GEO accession number: GSE153497. The calculation of frameshift index for each gene was performed as described above, with the only modifications of using *in-frame* reads at position -14 (F1) and the *out-of-frame* reads at position -15 (F0) due to the difference of ribosomal fragment protection size between yeast and bacteria. Transcripts with greater than 30 reads and 10 reads per million (rpm) were considered for subsequent analysis in each biological replicate.

Gene-specific frameshift index for *B. subtilis* 168 and *L. plantarum* were computed as follows: $\log_2(F1/F0)_{control} > 0$ and $\log_2(F1/F0)_{treatment} < 0$. Statistical analysis for frameshift index distribution between two populations was performed with a Kolmogorov–Smirnov test.

To infer codon optimality in *B. subtilis* 168 and *L. plantarum*, we obtained tRNA adaptation index and Codon adaptation index from Perach et al.⁴² and Fuglsang⁴¹ respectively.

All clustering analyses and heatmap were performed by k-means using Complexheatmap packages from R and Bioconductor.⁶⁰ Gene Ontology enrichment analysis was performed with ClusterProfiler⁶¹ using Fisher's exact test with p adjusted value < 0.05 . Datasets for *S. cerevisiae* tRNA adaptation index, mRNA codon stability index, translation efficiency were obtained from Carneiro et al.,⁶² gene expression level, mRNA half-life, 3'/5' UTR length and GC contents were obtained from Xu et al.,⁶³ Presnyak et al.,¹⁰ Pelechano et al.⁶⁴ and Latorre et al.⁶⁵ respectively.

SLAM-seq metabolic labeling

Metabolic labelling of newly synthesized RNA molecules was performed as previously described.^{30,66,67} Briefly, 4-Thiouracil (4tU, Sigma) was dissolved in NaOH (83 mM) used for labelling RNA molecules. The final concentration of 4tU for YPD and CSM was 5 mM⁶⁶ and 0.2 mM,⁶⁷ respectively. MES buffer (pH 5.9) with a final concentration of 10 mM was prepared with media to avoid the pH change due to 4tU addition. Wildtype (BY4741), NMD mutant (*upf1*Δ), *dcp2-7*Δ, *dhh1*Δ, *gcn1*Δ, *gcn1upf1*Δ were used for these experiments. To perform pulse and chase experiment, RNA molecules were labelled with 4tU (prepared as above) for 1h during cell

growth at mid exponential phase. Cells were washed and resuspended in prewarmed medium (YPD with MES buffer or CSM with MES buffer) without 4tU and time points were collected at 0, 15 and 30 mins by centrifugation and snap frozen in liquid nitrogen immediately.

To perform thiol(SH)-linked alkylation, the reaction including 5 µg of RNA was incubated with iodoacetamide (final concentration at 0.5 M) at 50°C for 15 minutes.³⁰ The reaction was stopped by adding 0.1 M DTT (final concentration at 20 mM). RNA was then precipitated by 3 M of sodium acetate and pure ethanol. Purified RNA was subjected for ribosomal RNA depletion using RiboPools Depletion Kit (siTOOLS Biotech). Libraries were prepared by Ultra™ II Directional RNA Library Prep Kit for Illumina® following manufacturer's instructions. Sequencing was performed on Illumina Nextseq 2000 sequencer with single end read length for 150 cycles.

SLAM-seq data analysis

SLAM-Seq data analysed was performed with slamdunk (v0.4.3) provided by nfcore pipeline(v1.0.0)(<https://nf-co.re/slamseq>). Firstly, fastq compressed files (fastq.gz) were converted to reverse complementary reads method and feed into slamdunk nf core pipeline as stranded libraries were prepared with dUTP. Adapter contamination and low-quality bases were trimmed using TrimGalore(v 0.6.4) (trim length 27bp). Slamdunk was used for mapping, quantifying nucleotide-conversions and collapsing quantifications on gene level. At least 1 T>C conversions per read was regarded as a confident call for labelled RNA reads. Genes with less than 20 reads were filter out. SNP masking was employed to distinguish filter T>C SNPs from converted nucleotides. T > C reads counts in each library were normalized to total library read counts. Normalized T > C reads counts across time were fitted to non-linear decay model equations with R function nls to calculate degradation rate for each condition:

$$y \sim C * \exp(-a * t_m)$$

where normalized T > C reads counts fitted to y, with chasing time points from 0, 15 and 30 mins being fitted to t_m . The model was used to estimate parameters C and a, from which the RNA half-life was calculated as $\log_2(a)$. Degradation rate was calculated as $60 * \ln(2) / t_{1/2}$ ($t_{1/2}$ is half-time of gene). To show the percentage of labelled read across time, T>C conversions were normalized to chase-onset (t_0). Only samples with more than 1,000 detected genes and reliable RNA degradation rate estimates were retained for subsequent analysis. Environmental decay-sensitive genes are defined according to degradation rate in wildtype and mutant: degradation rate (wt/mutant Δ)_{CSM} > 1.2 and (wt/ mutant Δ)_{YPD} < 0.8).

Ribosome profiling library preparation

Yeast overnight cultures were diluted to OD₆₀₀ 0.05 in 1000 ml CSM medium and grown at 30 °C. All cells were collected by vacuum filtration and freezing by liquid nitrogen. To perform lysis, 200 µl glass beads and 500 µl of freshly prepared lysis buffer (composed of 20 mM Tris pH 8.0, 140 mM KCl, 1.5 mM MgCl₂, 1% Triton X-100, 0.1 mg/mL cycloheximide, 2 mM DTT, and an EDTA-free protease inhibitor tablet) were added. Cells were pulverized by vortexing using a Multimixer for 2 minutes, followed by a 5 minute incubation on ice. This process was repeated three times to maximize the yield of RNA. After adding an additional 200 µl of lysis buffer to compensate for volume loss, the lysate was then centrifuged at 3000 g for 5 minutes at 4°C. After quantifying RNA concentration, 200 µg RNA was incubated with 2 µl 100 U/µl RNase I (Ambion) for 1 h at 22 °C with gentle agitation (700 rpm) and the reaction was inhibited by the addition of 15 µl Superaseln (Thermo Fisher). Another 50 µg RNA from the lysate was kept on ice undigested to use for polysome profiles. Linear sucrose gradient centrifugation and fractionation were then performed as described previously,⁶⁸ except we modified the 10X sucrose gradient buffer (consisting of 0.5 M Tris-Acetate pH 7.0, 0.5 M NH₄Cl, and 0.12 M MgCl₂) to make it suitable for yeast cells. RNA was extracted in 20 mM Tris-HCl (pH 7.5), 300 mM sodium acetate, 2 mM EDTA, 0.25% SDS overnight at room temperature with rotating and then precipitated. Monosome fraction RNA was isolated by the standard phenol: chloroform method. RNA footprints were isolated at 20-35 nucleotide size using 15% TBE-urea gel. To further ligate 3' and 5' adapters, RNA samples were treated with PNK to obtain 5' phosphorylated and 3' hydroxylated ends, followed by ribosomal RNA depletion by using the RiboPools Depletion Kit (siTOOLS Biotech). For total RNA, ribosomal RNA was depleted (as described above) followed by fragmentation with magnesium at 80°C for 5 mins. RNA samples were treated with PNK to obtain 3' hydroxylated ends for further 3' ligation. Monosome RNA footprints and total RNA were prepared using a Small RNA Sample Preparation Kit for NEXTFLEX® following manufacture instructions. Sequencing was performed with single end setting, read length 47 bp on Illumina Nextseq 2000 sequencer.

Ribosome profiling data analysis

Ribosome profiling data was trimmed using cutadapt and the following parameters: -a TGG AATTCTCGGGTGCCAAGG. To keep the minimum length, the cutoff set to 10 nt. After that the 4-nt random barcodes from both 5' and 3' ends of reads were extracted as UMIs. Ribo-seq reads and RNA seq reads were selected at 28-32 nt and 20-70 nt, respectively. Reads were mapped to reference genome (SGD R64-1-1) using star/2.7.0. Analysis of 5' end positions was performed using *Fivepseq* package as described above. The distribution of frames with respect to the size of the ribosome-protected fragments were determined using the riboSeqR package in R (v4.0.4).

Ribosome profiling data for amino acid deprivation in human cell lines was obtained from Loayza-Puch et al.⁴³ with GEO accession number: GSE59821. Ribosome profiling data were adapter trimmed using cutadapt by the following parameters: -a AAAAAAAAAA -minimum-length=13. Reads were mapped to reference genome (GRCh38) using star/2.7.0. Analysis of 5' ends positions was performed using *Fivepseq* package as described above. The calculation of frameshift index for each gene were described above, with

modifications as follows: 1) using in-frame reads at position -17 (F1) and the out-of-frame reads at position -18 (F0) according to human ribosome protection fragment size. 2) Only genes whose length was divisible by 3 and whose coding sequence (CDS) started with ATG and ended with either TAG, TGA, or TAA stop codons were considered. Codon optimality data was downloaded from Forrest et al.⁴⁴

Dual-fluorescent frameshifting assays

To construct the frameshift reporters, we designed test sequences containing programmed frameshifting regions (PRF), mutated PRF sites, and stretches of proline and arginine codons. These sequences were inserted between Red Fluorescent Protein (RFP) at the 3' end and Green Fluorescent Protein (GFP) at the 5' end, synthesized with *SpeI* and *XhoI* restriction sites at their 5' and 3' ends, respectively (sequences provided in Table S4). The four resulting constructs were digested with *SpeI* and *XhoI*, cloned into the p416-TEF plasmid, and transformed into BY4741 yeast cells. After isolating individual colonies, successful integration was confirmed by Sanger sequencing (primers listed in Table S4). For fluorescence measurements, cells were grown to exponential phase in an orbital shaker with appropriate medium, and cells grown in YPD were harvested and washed with PBS. Fluorescent activity was measured using a BMG plate reader according to manufacturer's specifications. For analysis, the background subtracted GFP signal was divided by RFP signal, and this ratio was normalized to the GFP/RFP ratio of the mutated PRF reporter to determine the frameshift rate.

To assess the impact of amino acid supplementation on frameshifting efficiency, we individually supplemented the growth medium with nine different amino acids: arginine, alanine, proline, histidine, leucine, lysine, serine, asparagine, and methionine. Each amino acid was supplemented at a concentration of 85.6 mg/L. The effect of amino acid supplementation on frameshifting was quantified by comparing GFP/RFP ratios between amino acid-treated and untreated samples, with measurements performed in 4 replicates for each condition.

Sample preparation for proteomics analysis

Yeast cells grown in YPD or CSM media were quenched by adding pure trichloroacetic acid (Sigma Aldrich) to the yeast cultures to a final concentration of 10% (v/v) and incubating for 10 min on ice. Samples were then centrifuged at 2500 g for 5 min at 4°C and the supernatant was discarded. The pellet was washed twice with 10 ml cold acetone before being transferred into a new tube. After an additional centrifugation step at 3000 g for 5 min at 4°C, the acetone was removed and the pellet was further processed for protein extraction.

Cell lysis and protein extraction for proteomics analysis

To lyse the cells, cell pellets were first mixed with glass beads (Sigma Aldrich) and 500 µl of lysis buffer containing 8M urea, 50 mM ammonium bicarbonate and 5 mM EDTA (pH 8). The mixture was then transferred to a FastPrep-24TM 5G Instrument (MP Biomedicals) where cells were disrupted at 4°C by 4 rounds of bead-beating at 30 seconds with 120 seconds pause between the runs. Samples were then centrifuged for 10 min at 21'000 x g to remove cell debris and the supernatants were transferred into a new tube. The protein concentration was determined using the bicinchoninic acid Protein Assay Kit (Thermo Scientific) following the manufacturer's protocol.

In-solution protein digestion for proteomics analysis

100 µg of protein extracts were subjected to digestion. Samples were vortexed and sonicated for 5 min. In the first step, dithiothreitol (Sigma Aldrich) was added to a final concentration of 5 mM and incubated for 30 min at 37°C to reduce the disulfide bridges followed by the alkylation of free cysteine residues with iodoacetamide (Sigma Aldrich) at 40 mM final concentration (30 min at 25°C in the dark). Samples were pre-digested with lysyl endopeptidase (Wako Chemicals) at an enzyme substrate ratio of 1:100 for 4 h at 37°C and then diluted 1:5 with freshly prepared 0.1 M ammonium bicarbonate to reduce urea concentration to 1.6M. Sequencing grade trypsin (Promega) was added at an enzyme substrate ratio of 1:100 and digested at 37°C for 16h. The digestion was stopped by adding formic acid (Sigma Aldrich) to a final concentration of 2%. The digested samples were loaded onto SepPak C18 columns (Waters) that were previously primed with 100% methanol, washed with 80% acetonitrile (ACN, Sigma Aldrich), 0.1% FA and equilibrated 3 times with a 1% ACN, 0.1% FA solution. The flow-through was loaded once more onto the columns and the peptides bound to C18 resins were afterwards washed 3 times with a 1% ACN, 0.1% FA solution and eluted twice with 300 µl 50% ACN, 0.1% FA. The elution was dried down in a vacuum centrifuge and peptides were resuspended in a 3% ACN, 0.1% FA solution to a concentration of 1 mg/ml before liquid chromatography mass spectrometry (LC-MS) analysis.

Liquid chromatography-mass spectrometry for proteomics analysis

Peptide samples were analysed in a Data-Independent Acquisition mode (DIA) with an Orbitrap Exploris 480 mass spectrometer (Thermo Fisher Scientific) equipped with a nano-electrospray ion source and a nano-flow LC system (Easy-nLC 1200, Thermo Fisher Scientific). Peptides were separated with fused silica capillary column (25 or 50 cm) with inner diameter of 75µm packed in house with 1.9 µm C18 beads (Dr. Maisch Reprosil-Pur 120). For LC fractionation, buffer A was 3% ACN and 0.1% FA and buffer B was 0.1% FA acid in 90% ACN and the peptides were separated by 2 h non-linear gradient at a flow rate of 250 nl/min with increasing volumes of buffer B mixed into buffer A. The DIA-MS acquisition method consisted of a survey MS1 scan from 350 to 1650 m/z at a resolution of

120,000 followed by the acquisition of DIA isolation windows. A total of 40 variable-width DIA segments were acquired at a resolution of 30,000. The DIA isolation setup included a 0.5 m/z overlap between windows.

Quantitative proteomics data analysis

DIA-MS measurements were analysed with Spectronaut 16 (Biognosys AG) using direct searches. In brief, retention time prediction type was set to dynamic iRT (adapted variable iRT extraction width for varying iRT precision during the gradient) and correction factor for window 1. Mass calibration was set to local mass calibration. The false discovery rate (FDR) was set to 1% at both the peptide precursor and protein level. Digestion enzyme specificity was set to Trypsin/P and specific. Search criteria included carbamidomethylation of cysteine as a fixed modification, as well as oxidation of methionine and acetylation (protein N-terminus) as variable modifications. Up to 2 missed cleavages were allowed. The DIA-MS files were searched against the *Saccharomyces cerevisiae* proteome (UniProt version 2021-04-02). Differentially regulated proteins were determined with an unpaired t-test statistic with correction for multiple testing with the Storey method correction. After quantification of protein abundance, the proteins that were upregulated and downregulated were identified based on \log_2 (CSM/YPD) values >1 and < -1 , respectively. Additionally, a Q-value of less than 0.01 was used as a criterion for selection. Volcano plot for protein abundance comparison was plotted using the EnhancedVolcano package from R. Gene set enrichment analysis (GSEA) for proteins was performed with ClusterProfiler⁶¹ using Fisher's exact test with p adjusted value < 0.05 . Protein-protein interactions were performed by metascape⁵⁹ v3.5 with p adjusted value < 0.05 .

QUANTIFICATION AND STATISTICAL ANALYSIS

All statistical analyses were performed using R (version 4.0.4). Specific tests are indicated in figure legends and the methods section. Significance is denoted as: unlabeled or ns ($p > 0.05$), * ($p \leq 0.05$), ** ($p \leq 0.01$), and *** ($p \leq 0.001$). Bar graphs show mean \pm SEM or SD as indicated. Student's t-tests and wilcoxon rank sum tests were performed in R.

Graphical abstract Created in BioRender. Pelechano, V. (2025) <https://BioRender.com/e96v507>.